DISCLAIMER

This report was prepared as an account of work sponsored by an agency of the United States Government. Neither the United States Government nor any agency thereof, nor any of their employees, makes any warranty, express or implied, or assumes any legal liability or responsibility for the accuracy, completeness, or usefulness of any information, apparatus, product, or process disclosed, or represents that its use would not infringe privately owned rights. Reference herein to any specific commercial product, process, or service by trade name, trademark, manufacturer, or otherwise does not necessarily constitute or imply its endorsement, recommendation, or favoring by the United States Government or any agency thereof. The views and opinions of authors expressed herein do not necessarily state or reflect those of the United States Government or any agency thereof. Reference herein to any social initiative (including but not limited to Diversity, Equity, and Inclusion (DEI); Community Benefits Plans (CBP); Justice 40; etc.) is made by the Author independent of any current requirement by the United States Government and does not constitute or imply endorsement, recommendation, or support by the United States Government or any agency thereof.

SAND2026-18013

SANDIA REPORT
SAND20XX-XXXX
Printed Click to enter a date

Sandia National Laboratories

Bryan Mound Geomechanical Model Update

Kyung Won Chang

Prepared by
Sandia National Laboratories
Albuquerque, New Mexico
87185 and Livermore,
California 94550

Issued by Sandia National Laboratories, operated for the United States Department of Energy by National Technology & Engineering Solutions of Sandia, LLC.

Available to DOE and DOE contractors from
U.S. Department of Energy
Office of Scientific and Technical Information
P.O. Box 62
Oak Ridge, TN 37831

Telephone: (865) 576-8401
Facsimile: (865) 576-5728
E-Mail: reports@osti.gov
Online ordering: http://www.osti.gov/scitech

Available to the public from
U.S. Department of Commerce
National Technical Information Service
5301 Shawnee Rd
Alexandria, VA 22312

Telephone: (800) 553-6847
Facsimile: (703) 605-6900
E-Mail: orders@ntis.gov
Online order: https://classic.ntis.gov/help/order-methods/

ABSTRACT

This report presents computational analyses that simulate the structural response of caverns at the Strategic Petroleum Reserve Bryan Mound site. The cavern field comprises 20 caverns. Five caverns (BM1, 2, 4, and 5; BM3 was later plugged and abandoned) were acquired from industry and have unusual shapes and a history dating back to 1946. The other 16 caverns (BM101 to 116) were leached according to SPR standards in the mid-1980s and have tall cylindrical shapes. The history of the caverns and their shapes are simulated in a 3-D geomechanics model of the site that predicts deformations, strains, and stresses. Historical wellhead pressures are used to calculate cavern pressures up through January 2025. Because of the extent of heterogeneous creep behavior observed throughout the Bryan Mound site, a set of cavern-specific creep coefficients was developed to produce better matches with measured cavern closure. For this new implementation of the model, there are two significant advances: the use of the multimechanism deformation viscoplastic (MDV) salt creep model to integrate both steady-state and transient salt creep at low stress states; and the update of finite element mesh geometries for the caverns that nearly exactly match the geometries obtained through sonar measurements. The model has been built with several options to allow for exploration of different parameter and operations scenarios; these will be particularly useful if a recent advance in the calculation speed using the MDV model is fully realized. The geomechanical results of the updated finite element model are interpreted to provide information on the current and future status of cavern performance, cavern stability, and well integrity. More detailed evaluation of the effects of cavern pressure changes on stress behavior in the salt surrounding the cavern will lead to more accurate evaluation of long-term cavern integrity and evolution of drawdown availability.

ACKNOWLEDGEMENTS

The authors would like to thank Anna C. Snider Lord, Byoung Yoon Park, Tonya S.A. Ross, for their contributions to the work described in this report, and the U.S. Department of Energy, Strategic Petroleum Reserve office for their review and support of this work.

CONTENTS

This page intentionally left blank.

LIST OF FIGURES

This page intentionally left blank.

LIST OF TABLES

This page left blank

EXECUTIVE SUMMARY

This report presents he most recent computational analyses that simulate the structural response of caverns at the Strategic Petroleum Reserve Bryan Mound site. For this new implementation of the model, there are two significant advances. The first is the use of the multi-mechanism deformation viscoplastic (MDV) salt creep model to evaluate both steady-state and transient salt creep. The addition of the low-stress creep mechanisms enables to capture salt behaviors in response to steady-state stressing and transients such as cavern pressure changes. The second is the update of finite element mesh geometries for the caverns that nearly exactly match the geometries obtained through recent sonar measurements. The mesh construction for the caverns implements a patented process that creates a mesh geometry that matches nearly exactly the cavern geometry measured via sonars (Park et al., 2017 and 2018). This feature is particularly important for caverns with unusual geometric features, such as significant protuberances in Cavern 105. With two major upgrades of the Bryan Mound geomechanical model, the cavern-specific creep properties are re-calibrated based on the field measurement of cavern volume changes and the potential of stress-related damage of caverns is re-evaluated. Other continuing features include the use of historical wellhead pressures to determine cavern pressures, separate regions of hard and soft salt on either side of a prominent boundary shear zone, separate regions of caprock which are undamaged or damaged by steam-injection sulfur mining in the early 20th century, and the inclusion of five full-drawdown leach layers for near all the caverns.

The results of the computational analyses lead to the following conclusions regarding the model itself, and the conditions of the caverns at Bryan Mound:

- The set of salt creep model properties for the new MDV model is re-calibrated, and the new model results of cavern volume change matches CAVEMAN-derived closure data much better than the previous Bryan Mound models.
- The inclusion of the low-stress creep mechanisms and update of realistic cavern geometries to the computational mesh result in changes of stress conditions corresponding to the cavern operation history.
- A sensitivity test with variation in caprock mechanical property shows that the caprock is squeezed in a vertical direction resulting from the expansion of the pressurized cavern and dome above the operating cavern. This geomechanical simulation result is consistent with the field observation of wellbore failure within a caprock region above BM116, potentially driven by compression in a vertical direction.
- The potential of stress-related damage based on the evolution of dilatant and tensile stresses around certain caverns needs to be re-evaluated through planned workover and drawdown activities.

The new model represents a more realistic assessment of the behavior of the Bryan Mound site. However, uncertainty still exists regarding several aspects of the model, and how they pertain to operational issues at the site. The types of uncertainty include the following items which will be addressed in future work:

- Implementing hydrological and mechanical properties of the caprock measured from the laboratory tests on core samples from the Bryan Mound site.

- Using the existing mesh but implementing different workover scenarios to test hypotheses of observed sympathetic behavior in one cavern when a nearby cavern undergoes a workover.
- Adding an actual well structure into the current computational domain and/or developing a local model to investigate the location-specific geomechanical behavior of the cavern and surrounding formation.
- Creating differently-shaped "onion skin" layers based on sonars or SANSMIC simulations will illustrate the leaching effects of partial drawdowns, which are much more the normal operating mode than a full bottom-to-top drawdown. Such partial drawdown scenarios will be important for providing guidance to the DOE for tracking the available drawdown capacity for each cavern.

ACRONYMS AND TERMS

Acronym/Term	Definition
ASC	Advanced Simulation and Computing
BM	Bryan Mound
DOE	Department of Energy
MDC	Multi-mechanism Deformation Creep
MDV	Multi-mechanism Deformation Viscoplastic
Sierra/SM	Sierra/SolidMechanics
SNL	Sandia National Laboratories
SPR	Strategic Petroleum Reserve

1. INTRODUCTION

1.1. Objective

The U.S. Department of Energy (DOE) Strategic Petroleum Reserve (SPR) stores crude oil in solution-mined caverns in the salt dome formations of the Gulf Coast. There is a total of 60 caverns located at four different sites in Texas (Bryan Mound and Big Hill) and Louisiana (Bayou Choctaw and West Hackberry), as shown in Figure 1. Each cavern is constructed by drilling one or more boreholes into the salt dome and injecting fresh water. The fresh water dissolves the salt and creates brine, which is then pumped out of the cavern. This process, which is known as leaching, creates a brine-filled volume in the salt that is eventually used for the storage of oil. The boreholes (or wells) of the cavern are then lined with steel casings cemented in place from the surface to near the top of the cavern. The safe and effective operation of the storage caverns requires technical issues to be addressed in order to maintain the integrity of the caverns and their wells. The Bryan Mound salt dome, located approximately 60 miles south of Houston, Texas, near the city of Freeport, is the largest of the SPR sites in terms of oil-storage capacity (currently 226 million barrels). Sandia National Laboratories (SNL), as the geotechnical advisor to the DOE SPR Project Office, conducts site-characterization investigations and other longer-term geotechnical and engineering studies in support of the program.

The SPR sites, as well as most other oil and natural gas storage sites in salt domes along the Gulf Coast, are varied in terms of cavern structure and layout. The Bryan Mound SPR site was acquired by DOE, by condemnation, in April 1977 from the Freeport Mineral Company and other owners. At that time there were five caverns at the site. An analysis of these existing Phase 1 caverns from 1977 to 1979 resulted in four of them, Caverns 1, 2, 4, and 5, being certified for crude oil storage. As early as October 1977 oil injection commenced at the site. After purchase of the site, additional caverns were leached using standards that resulted in tall cylindrical shaped caverns; these caverns, numbered 101 through 116, are referred to in this report as Phase 2 or post-1981 caverns. The Bryan Mound salt dome includes at least three boundary shear zones, which tend to divide the dome into zones of high and low salt creep potential. However, creep rates as measured by cavern closures vary significantly throughout the salt dome. Furthermore, sulfur mining in the caprock at Bryan Mound occurred in the early 20th century (Kirby and Lord, 2015). Sulfur mining was performed using the Frasch extraction method, for which superheated steam at 320°F was injected into the caprock to draw out sulfur, in a mostly molten form with some SO_2 and H_2SO_4. This mining method both weakens the in situ rock and removes material, and thus induces underground collapse and subsidence; in the case of Bryan Mound, evidence of this subsidence is indirect, with no known monitoring program. The one Phase 1 cavern not selected for oil storage, Cavern 3, was filled with brine, plugged and abandoned in 1980. The effect of its presence on surface subsidence and salt dome structural integrity has been analyzed in previous Sandia analyses of the Bryan Mound site (Sobolik and Ehgartner, 2009a, 2009b, 2012a & 2012b; Sobolik and Lord, 2014). Cavern 2 at Bryan Mound was decommissioned in 2016, with the oil removed and replaced with brine. The cavern is pressurized at normal operating pressure to maintain cavern integrity.

SNL has performed several previous analyses that model the behavior of the caverns in the Bryan Mound salt dome, and evaluate possible effects on site operations such as potential casing failures. The first analysis (Sobolik and Ehgartner, 2009) described three-dimensional (3-D) geomechanical calculations modeling the long-term behavior of the Bryan Mound SPR site in response to changing oil pressure conditions in the storage caverns and future growth of the caverns through subsequent leaching. The 2009 analysis also evaluated the stress and deformation history of the caverns to the

present day, and predicted the effects on cavern stability and well strain of subsequently enlarging the caverns. Those calculations used a computational mesh that included a geometrically-realistic rendition of the Bryan Mound salt dome, and sonar-based, axisymmetric representations of the vast majority of the oil storage caverns.

Figure 1. Locations of the four U.S. SPR sites (Bryan Mound, Big Hill, West Hackberry, and Bayou Choctaw).

Sobolik and Ehgartner (2009a) also assumed a homogeneous, elastic caprock layer, and a linear temperature distribution as a function of depth based on measurements from deep in the salt dome. Long-term cavern performance was evaluated using four performance measures: a dilatant damage criterion based on deviatoric stress; cavern volume closure; axial well strain in the caprock; and maximum surface subsidence above each cavern. Because of the large variability of salt creep properties throughout the Bryan Mound salt dome, there was a similarly large variability in the correlation between measured and predicted cavern closure and surface subsidence rates.

Sobolik and Ehgartner (2009a) predicted elongation along the boreholes casings and liners that resulted in axial strains in the caprock section not exceeding the prescribed threshold strains of 0.2 millistrains for cement and 1.6 millistrains for steel casings. They also predict axial strains in the salt that exceed the cement liner threshold value, but not the steel casing threshold. These analytical results came into question when several well casings at the Bryan Mound site experienced failures of various types. None of the documented failures appeared to be a joint separation due to excessive elongation, which would have been the type most expected. Instead, the failures appeared to be one of several varieties: outward bowing of the walls of the casing due to axial compression; intrusion of cement or steel into the wellbore; or shear failure due to horizontal shear or twisting stresses. These failures made it obvious that the caprock in which these casings are installed is not behaving as previously modeled, and that unusual stresses are being generated at the casings. Therefore, a new

analysis was conducted (Sobolik, 2010) for which a series of sensitivity studies was performed, altering the mechanical properties of selected sections of the caprock. These calculations were performed using a 30-degree wedge to simulate a symmetric 19-cavern field geometry, with the caprock divided into concentric sections to easily allow for some spatial variability of caprock mechanical properties. Sobolik (2010) identified regions of higher probability of casing damage in the caprock due to proximity to sulfur mining wells and temperature in the caprock and created a prioritization list for inspection of wells based on several factors.

The conceptual and computational model for this new set of calculations includes several changes that allow greater accuracy in the geometric representation of the caverns, an upgrade to the multi-deformation salt creep model, and several options for modeling different sections of the caprock with varying physical properties to account for the effects of sulfur mining and its resulting void formation.

1.2. Report Organization

This report is organized in the following fashion: Section 2 gives a brief description of the Bryan Mound cavern site to show the diversity of cavern geometries. Section 3 describes the analytical model, including the cavern designs, stratigraphy, material models and properties, and damage criteria used for the analyses. Section 4 shows the results of the calculations, including forecasting future mechanical behavior and identifies the potential of stress-related damage, as well as geomechanics-based estimate of the available drawdown number. Section 5 summarizes the results and provides concluding remarks.

2. SITE DESCRIPTION

The Bryan Mound salt dome, located approximately 60 miles south of Houston, Texas, near the city of Freeport, is the largest of the SPR sites in terms of oil-storage capacity (currently 226 million barrels). The geological characteristics related to the Bryan Mound site were first described by Hogan (1980). Neal et al. (1994) utilized the earlier work, together with additional information on dome geology, surrounding stratigraphy, and relevant environmental information, to update the dome characterization. Conversion of the two-dimensional databases from these earlier characterization reports formed the basis for the most recent reexamination by Stein and Rautman (2005) using modern three-dimensional methods for representation of the dome and its surroundings. While major aspects of the dome, caprock and surrounding strata defined by the earlier characterizations remain unchanged, the updated three-dimensional models of Stein and Rautman (2005) used more refined analysis of the data and produced models of the dome that differed slightly from the earlier models. The three-dimensional models also achieve a level of visualization clarity and graphical manipulation previously impossible. Finally, the Bryan Mound caverns have been extensively characterized and mapped in a sonar atlas prepared by Lord (2007).

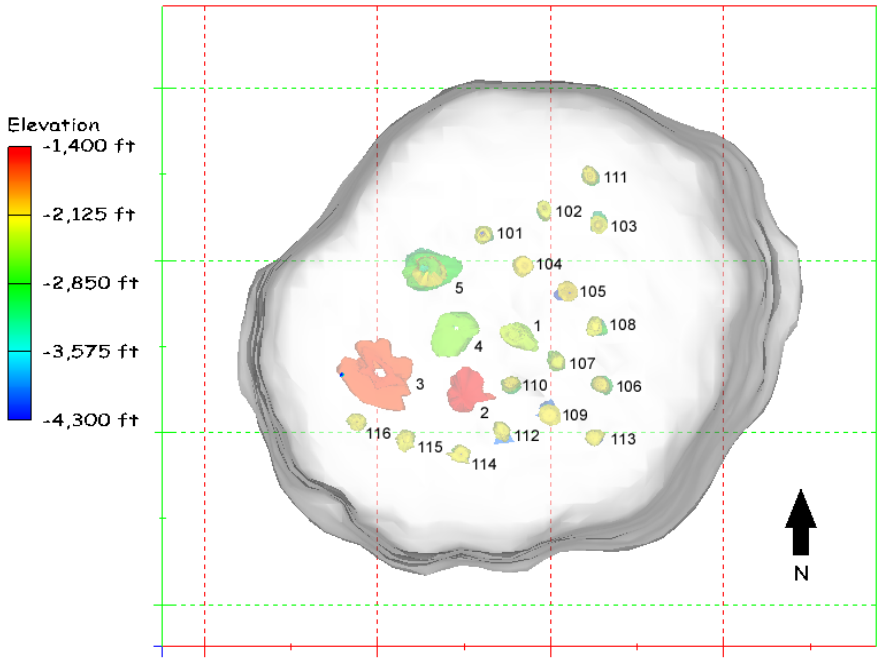

Figure 2. Top view of the Bryan Mound salt dome and caverns (Lord, 2007).

Figure 2 shows a plan view of the Bryan Mound site (Stein and Rautman, 2005) with the caverns' approximate location within the salt dome, and the interface of the salt dome with the caprock and surrounding sandstone. The approximate cavern locations are shown in the plan view. An updated geologic perspective of the salt dome and caprock are provided in Figure 3 (Lord, 2007). Note that there seem to be two regions within the salt dome that are possibly separated by a salt spine or shear zone. The thickest caprock regions correspond to the two separate regions inferred from the structure contour map.

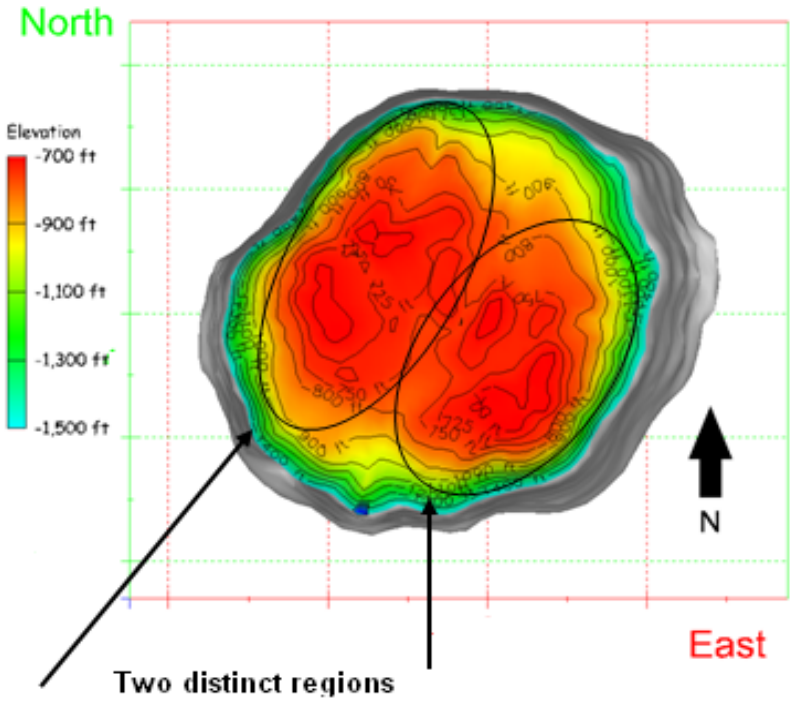

Figure 3. 3-D model of the top of caprock and the top of salt (considered to be the bottom of caprock); contours are of caprock elevation in feet (Lord, 2007).

Further study of the sonar data used to characterize the salt dome reveal the orientation of potential boundary shear zones within the salt dome; these zones are shown in Figure 4 (Lord, 2007). Of the three boundary shear zones shown in Figure 4, the one of greatest interest is that which is in the southeast portion of the salt dome, running roughly southwest to northeast. Caverns 106, 109, 112, 113, and 114 are located to the south of this shear zone. This region of the salt dome appears to contain salt with creep properties leading to higher creep rates than the remainder of the dome; Sobolik and Ehgartner (2009) took this into account and created a computational mesh with a salt dome along this shear zone. Cavern 3 can be seen in Figure 4 as the largest cavern at the western edge of the dome.

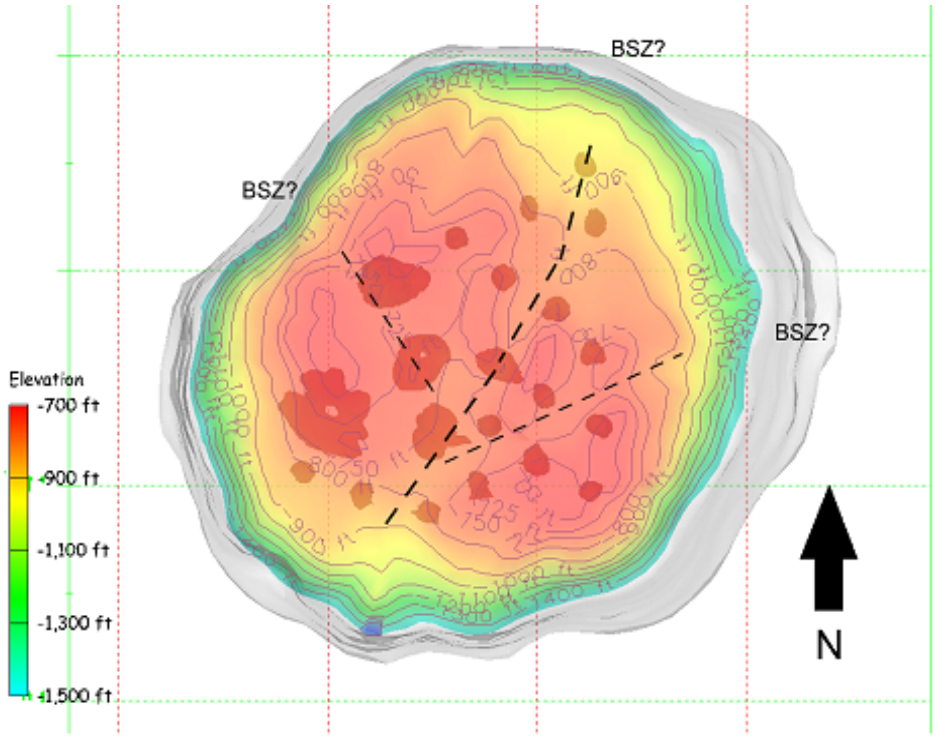

Figure 4. Potential boundary shear zones in the Bryan Mound salt dome (Lord, 2007b).

Figure 5 shows the cavern layout at the Bryan Mound site (Rautman and Lord, 2007), using the DOE coordinates provided; Cavern 4 is located in the cluster of cavern wells between caverns 1, 2, 3, and 5. Oil storage cavern geometries based on sonar measurements were obtained through 2007 (Rautman and Lord, 2007). Note the enlarged tops and asymmetries of the cavern shapes. In general, caverns in the SPR are intentionally shaped with larger tops to accommodate future oil drawdowns where only the bottom portions of the caverns are preferentially leached, and hence the overall cavern shape becomes more cylindrical, due to raw water injections to remove the oil. Salt properties also result in unpredictable cavern shapes as the insoluble content (primarily anhydrite) or dissolution rates of salt can spatially vary. This explains some of the asymmetries found in the cavern shapes. The Phase 1 caverns were acquired through purchase; these caverns have unusual shapes as they were not intentionally leached for product storage but were used to produce brine.

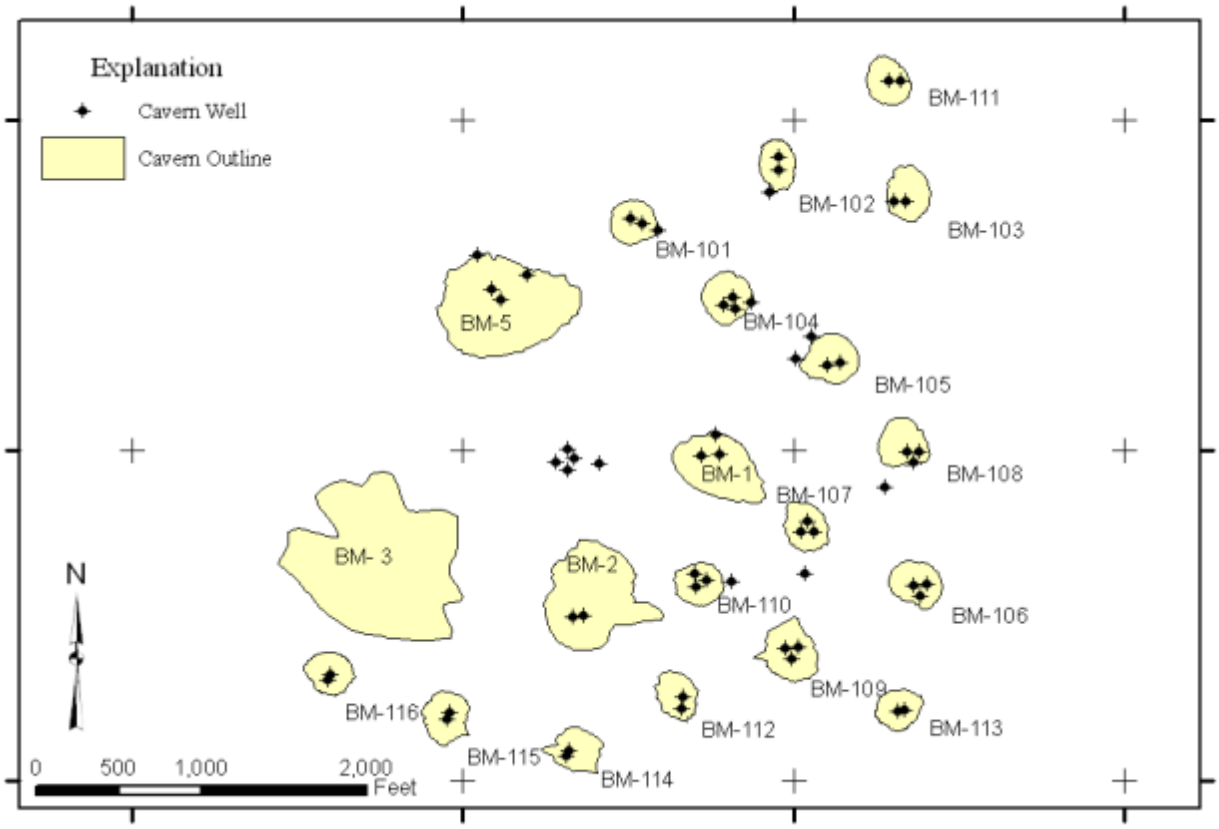

Figure 5. Schematic of the Location of the SPR Caverns at Bryan Mound (Rautman and Lord, 2007).

The Bryan Mound caprock was subjected to extensive sulfur mining prior to the development of the Strategic Petroleum Reserve. The caprock was mined in the 1910s-1920s using the Frasch technique, for which steam was injected into the caprock to leach out the sulfur to be pumped out to the surface. The long-term consequences of the sulfur mining include a large latent temperature perturbation in the caprock and upper 40-60 feet of the salt dome, the presence of sulfuric acid in the caprock, and significant volumes of void space from the removal of sulfur. These voids are the most likely explanation for lost circulation encountered in boreholes drilled into the salt dome during cavern formation. Figure 6 is an overlay map indicating the regions where most of the sulfur mining boreholes were drilled, and identifying the SPR caverns where lost circulation was encountered during drilling (Kirby and Lord, 2015).

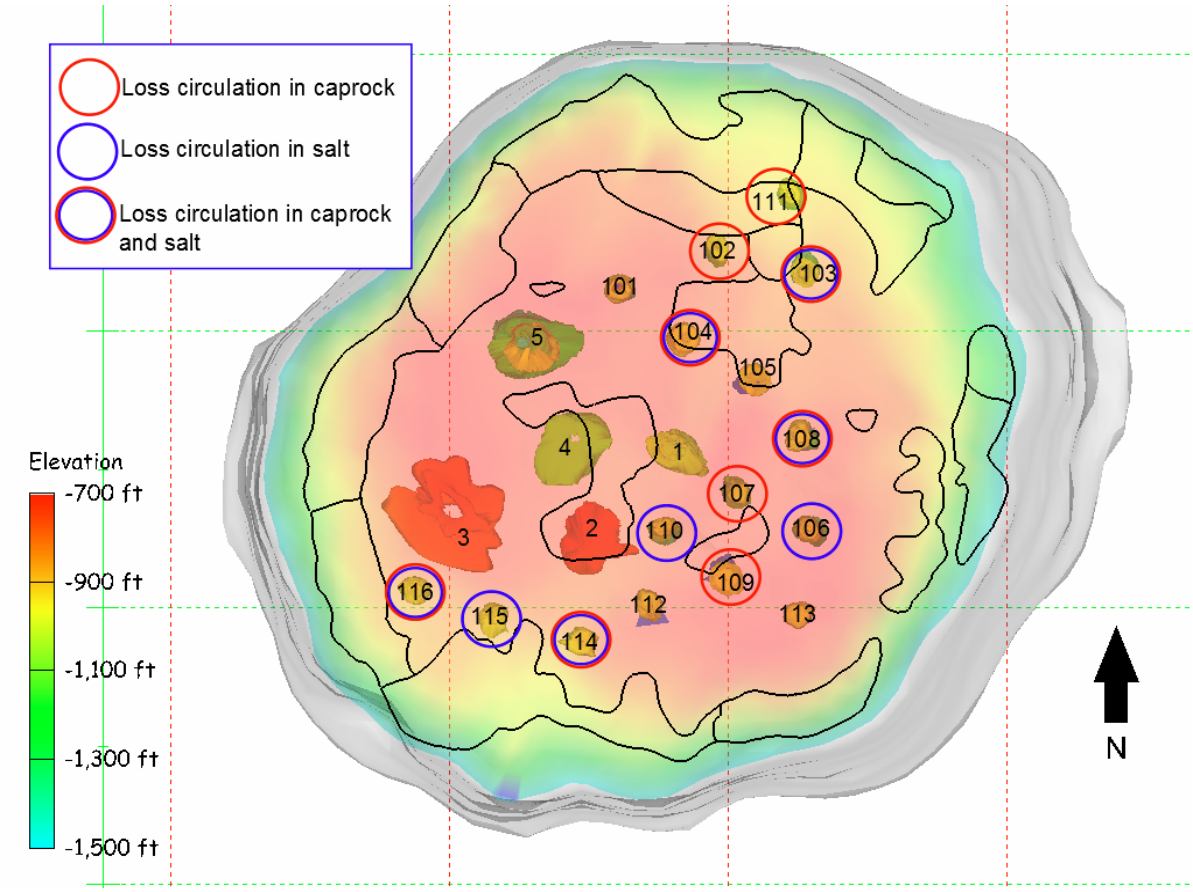

Figure 6. Plot of recorded cavern well loss circulation zones encountered during drilling.

Cavern 3, located in the southwestern quadrant of the dome (Figures 4 and 5), was initially developed by Dow in 1942 as one of five caverns in the Bryan Mound salt dome for brine production in the period 1942 to 1957. Four of these caverns (Caverns 1, 2, 4 and 5) were purchased by the DOE in 1977 and certified as suitable for oil storage by Gulf Interstate Engineering Company (GIEC). Cavern 3 was shut down in 1957 due to its large roof span. Cavern 3 contains a volume of 6.4 MMB based upon a 1979 sonar survey. The roof is highly irregular and the maximum diameter of the cavern (~1350') is the largest of any of the DOE owned caverns. About two years after it was shut down, the pressure dropped. Testing by Dow showed the well had hydraulic integrity, but not the cavern. The original 8-3/8" production casing failed in the mid-1950s, and a 5-1/2" in casing was cemented in. Dow believed the cavern was in communication with the top of salt. GIEC performed a number of tests (fluid level and brine sampling) and ran various cased hole logs in Cavern 3 in 1977. The cavern was not certified and the test results were not formally reported as were the results from the other caverns which were certified (Keplinger and Associates, 1980; Hogan, 1980). Brine samples taken at three different times between November 1977 and April 1978 showed significant variations in composition suggesting that circulation was occurring in the cavern. Later tests performed by Keplinger for SPR to determine freshwater circulation within the cavern were inconclusive, but the fact remained that the cavern did not hold pressure and therefore was not recommended for oil storage (Keplinger and Associates, 1980). Hogan (1980) and Preece and Foley (1984) performed computational analyses of Cavern 3. Both studies concluded that Cavern 3 was structurally stable, and neither study predicted tensile stresses in the roof of the cavern. Neither study indicated that Cavern 3 was hydraulically stable, and both

studies agreed with the recommendation that Cavern 3 should not be used for oil storage. Additionally, three surveys of the wells at Cavern 3 noted the presence of a void in the caprock of several feet in height at around 818 feet depth, and the height of the void decreased in succeeding reports (Keplinger and Associates, 1980 included the latest of these surveys). This void in the caprock has been assumed to have resulted from the sulfur mining at Bryan Mound.

3. ANALYSIS MODEL

3.1. Model Description

This analysis uses much of the same mesh generation and simulation methodologies as were used for previous analyses of Bryan Mound (Sobolik and Ehgartner, 2009a, 2009b, 2012a & 2012b; Sobolik and Lord, 2014). The new model includes many new enhancements involving the following elements:

- Mesh construction for the new model implements recent sonar-based geometries of caverns that captures nearly exactly the cavern geometry measured via sonars. This is described in Section 3.2.
- Mesh construction for the caprock creates zones in the caprock that match the mapped areas of sulfur mining illustrated in Figure 6. This construction allows for the option of performing multiple simulations in which the material properties of the mined areas may be modified to evaluate the effects of borehole casings throughout the site. This mesh development is described further in Section 3.2 and the caprock integrity analysis is described in Section 4.2.
- An improved implementation of the M-D viscoplastic (MDV) model in Sierra/Adagio, which is described in Section 3.3.
- The use of historical cavern pressures in the simulation, so that predicted cavern closure and surface subsidence results may be more directly compared to site data. This comparison was used to develop a set of cavern-specific creep properties for this analysis; this process and those properties are described in Section 3.4.
- Material properties used for the non-salt materials are described in Section 3.5, and the use of a dilatant stress damage factor (safety factor) is described in Section 3.6.

The history of the caverns is an important component of the model. At the Bryan Mound site, the five caverns known as Phase 1 – Caverns 1 through 5 – were created as early as 1946 and were used for brining and storage before the SPR took ownership of them in 1981. Cavern 3 was eventually filled with brine, plugged and abandoned. The analysis simulates the leaching of these caverns to full size over one year each, then filled with brine until 1981 and afterward filled with oil. Beginning in 1981, sixteen other storage caverns were created over a seven-year period. The analysis also simulates the leaching of the post-1981 caverns and subsequent filling with oil. In general, these caverns are maintained at constant operating pressure ranges except during workovers. The default pressure condition applied to each cavern is based on an average wellhead pressure ranging between 900 and 975 psi. For the simulation of cavern pressures during the life of the site, three stages are defined: the years prior to 1990, for which no wellhead pressure data were saved and so an estimate is made; the period between 1/1/1990 and 7/26/2016, for which historical data are used; and the future beyond 2016, for which the same algorithm from the first stage is used. For the first pressure stage beginning in the simulation year 1984, a series of five-year cycles of cavern workovers was initiated. During the five-year cycle, every cavern is scheduled for a workover. During the workover, the affected cavern is held at 0 psi wellhead pressure for three months. The pressures for all caverns are at normal operating pressure for the fourth month (so that the workover rig can be moved to a new well) and then the workover of the next scheduled well begins. Previous analyses have shown that the abrupt pressure drop during the workover are the times for greatest potential for damage to the cavern wall and borehole casings. The duration of the simulated workover may be slightly longer than is typically encountered in the field, but is chosen to provide an adverse

condition and closely simulate actual subsidence measurements, which reflect periods of low to intermediate operating pressures associated with fluid transfers. During the historical pressure period, workovers are reflected in the data during the times that the wellhead pressure is near zero.

3.2. Stratigraphy and Computational Mesh

The mesh developed for the computational model is illustrated in Figure 7. This mesh simulates the entire salt dome geometry and contains 7.9 million elements. Six material blocks are used in the model to describe the stratigraphic layers: the overburden, unmined and mined sections of the caprock, two sections of the salt dome designated "hard" and "soft" salt based on observed creep deformation rates, and the rock layers surrounding the salt dome.

The overburden is made of sand, and the caprock layer is made of gypsum or limestone. The overburden and caprock thicknesses are reasonably constant over the entire salt dome, so for meshing purposes they have been given constant values (Neal et al., 1994; Lord, 2007); the overburden layer is 760 feet thick, and the caprock 280 feet thick. However, certain sections of caprock comprising the bottom 100 feet of the layer and matching the lost circulation zones in Figure 6 were created as a separate material block so that the effects of weakened caprock in that section may be evaluated. The rock layers surrounding the salt dome comprised several layers of sandstone and shale; they have been modeled as one large layer of sandstone due to the minimal deviation in densities and rock mass moduli throughout those layers.

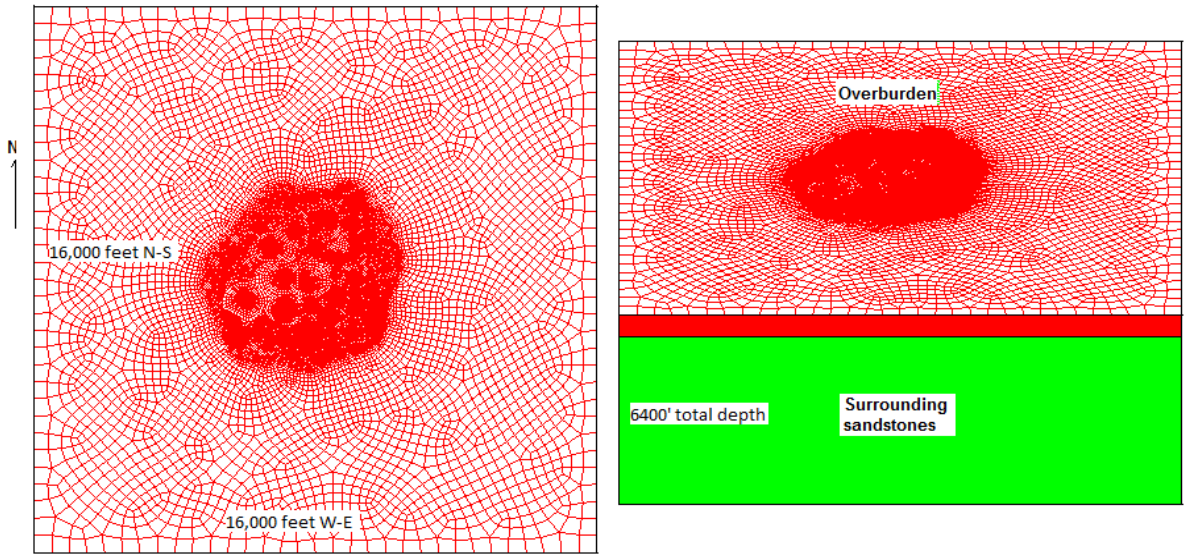

Figure 7. Computational mesh developed for the Bryan Mound calculations.

The Bryan Mound caprock was subjected to extensive sulfur mining prior to the development of the Strategic Petroleum Reserve. The caprock was mined in the 1910s to 1920s using the Frasch technique, for which heated steam at 160°C was injected into the caprock to leach out the sulfur, in a mostly molten form with some SO_2 and H_2SO_4, to be pumped out to the surface. The long-term consequences of the sulfur mining include a large latent temperature perturbation in the caprock and upper 40 to 60 feet of the salt dome, the presence of sulfuric acid in the caprock, and significant volumes of void space from the removal of sulfur. The voids may be in the form of new or enlarged pores, similar but larger vugs, or in new or expanded fractures, which are the most likely explanation for lost circulation encountered in boreholes drilled into the salt dome during cavern

formation. Also, the sulfur was not removed uniformly through the caprock because the large majority of the sulfur mining wells are located around the rim of the salt dome. Such a non-uniform damage pattern in the caprock may affect the spatial distribution of high stresses and strains. These factors can introduce mechanical, thermal and chemical environments that impact the long-term integrity of boreholes in the caprock and upper dome.

For this computational study, the numerical model assumes that the caprock thickness is reasonably constant over the entire salt dome (280 ft thick). Sections of caprock domain, comprising the bottom 100 ft of the layer, were constructed to represent the lost circulation zones weakened by steam-injection sulfur mining ("mined" or "damaged" caprock). Figure 8 shows the numerical domain of the Bryan Mound model for the caprock and salt formations; (A) the entire caprock and salt formation and (B) top view with the unmined/undamaged caprock removed to expose the mined/damaged caprock, salt dome and caverns with the cylindrical modeling columns.

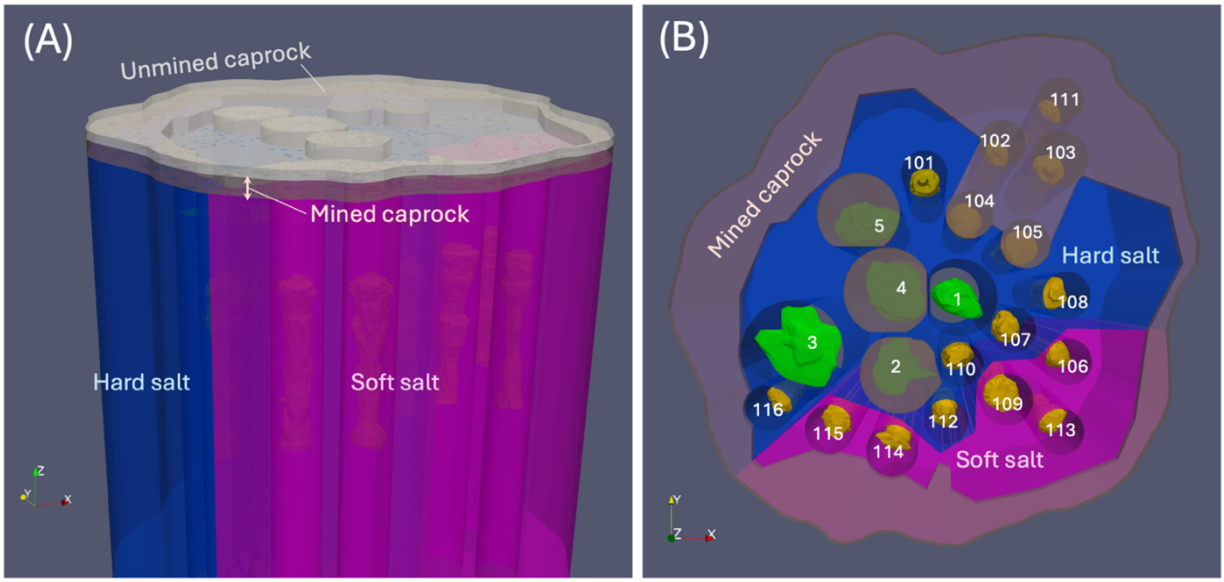

Figure 8. Numerical domain of the Bryan Mound geomechanical model. (A) the entire caprock (mined/damaged and unmined/undamaged) and salt formation (hard and soft) and (B) top view of the mined caprock, salt dome and caverns within the cylindrical columns. The unmined caprock region is opted out to visualize the location of caverns and salt dome.

Sobolik and Ehgartner (2009a) determined that the Bryan Mound salt dome would be best modeled by dividing it into "hard" and "soft" sections, based on the observed cavern volume closures at the site and on the existence of the shear zone boundary (refer to Figure 4). Figure 9 shows the top view of the meshed BM salt dome and cavern placement within the dome used in the geomechanical simulation. Two sections of the salt dome are designated "hard" and "soft" salt based on observed creep deformation rates (related to cavern volume closure); the full computational mesh includes the rock layers surrounding the salt dome.

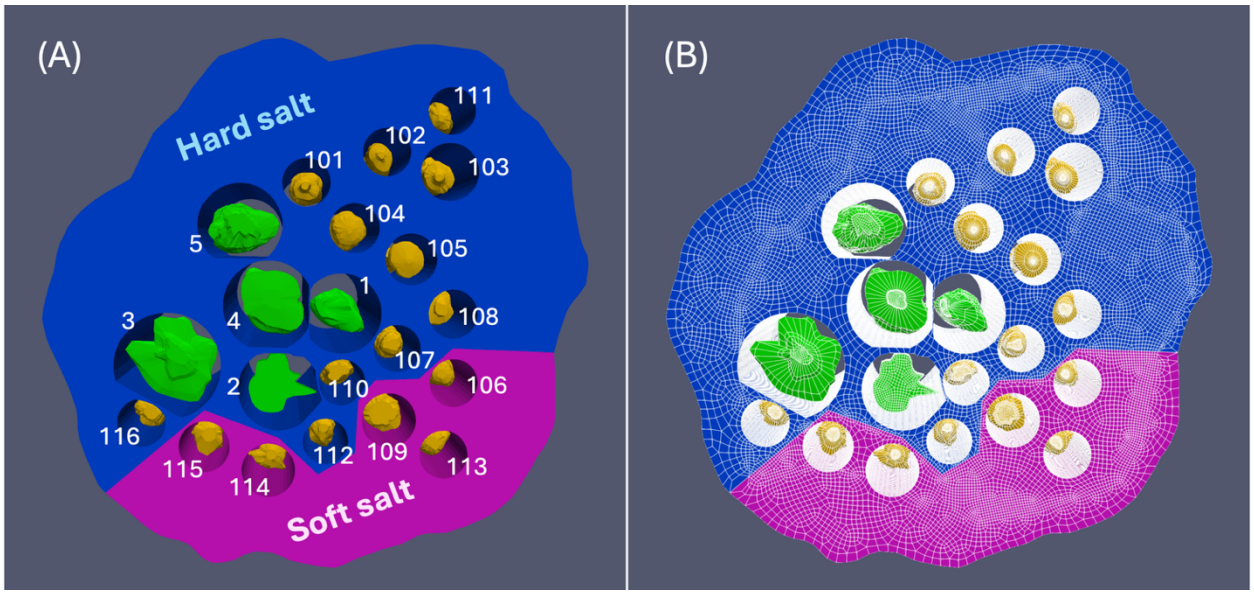

Figure 9. Top view of the numerical domain for salt dome and caverns. (A) Hard and soft regions in a Bryan Mound salt dome and (B) mesh for the domain. Note that the spaces between caverns and surrounding dome are null to show the cavern geometry.

The Bryan Mound geomechanical model has total 21 caverns with a salt dome as shown in Figure 9B. Caverns 1 through 5 (Phase 1 caverns) were initially developed by Dow in 1942 for brine production in the period 1942 to 1967, and have very irregular shapes. Caverns 1, 2, 4 and 5 were purchased for the SPR in 1977 while Cavern 3 was shut down in 1967 due to it is large roof span and permanently plugged and abandoned in 1988. Caverns 101 through 116 (Phase 2 caverns) were constructed by solution mining between 1981 and 1984 for oil storage, and have the typical tapered cylindrical shape. Caverns 106, 109, 112, 113 and 114 are located to the south portion of the salt dome, divided by one of the three boundary shear zones running roughly southwest to northeast (Lord, 2007). This region of the salt dome appears to contain salt with creep properties leading to higher creep rates than the remainder of the dome (referred to as the "soft" salt; magenta area in Figure 9) (Sobolik, 2018). The post-1981 Phase 1 caverns were typically constructed on 750-feet center-to-center spacings. Table 1 lists the cavern coordinates, top-of-cavern depths, and initial heights and volumes used in the analysis. The coordinates are based on Texas field coordinates, and converted to mesh coordinates with Cavern 1 at the origin, and coordinate axes aligned with compass directions (X-axis for W-E, Y-axis for N-S).

The construction of the finite element mesh for the caverns implements a new process that creates a mesh geometry that matches nearly exactly the cavern geometry measured via sonars (Park et al., 2017 & 2018). The Sandia mesh generation program CUBIT is used to create the mesh (Blacker et al., 2016). This process utilizes the fact that sonar data are usually taken at intervals of 20 feet as the instrument goes downward in the cavern. The geometry of these 20-foot sections forms the boundaries of the cavern mesh for the corresponding 20-foot sections. A mesh is generated for that section, and the nodal geometry for the individual elements is smoothed to produce the highest-quality hexahedral (6 sides, 8 nodes) elements possible using algorithms within CUBIT. The nodal geometry generated on the bottom of one 20-foot section is used for the nodal geometry on the top of the underlying section, thus maintaining nodal integrity throughout the mesh.

Table 1. Cavern coordinates, depths, heights, and construction dates used in the model.

Bryan Mound Cavern	X, feet (positive X is West)	Y, feet (pos. Y is North)	Depth to Ceiling, feet	Initial Height, feet	Initial Volume, MMB (1993)	Begin Construct (approx)	End Construct (approx)	Begin Oil Storage (approx)
1	0	0	2349	413	8.46	1/1/1946	1/1/1947	10/1/1978
2	-829.881	-988.094	1450	220	6.32	1/1/1946	1/1/1947	2/1/1978
4	-904.481	23.80583	2495	581	20.68	1/1/1946	1/1/1947	1/1/1978
5	-1334.58	924.5058	2102	1171	37.87	1/1/1957	1/1/1958	1/1/1984
101	-546.781	1415.506	1998	2161	11.23	9/1/1982	9/1/1984	9/1/1984
102	347.2786	1785.598	2203	2034	11.52	1/1/1981	5/1/1984	5/1/1984
103	1116.697	1518.731	2122	2011	11.43	5/1/1982	5/1/1984	5/1/1984
104	70.43307	942.4114	2108	2055	11.7	1/1/1981	1/1/1983	1/1/1983
105	716.3358	544.0781	2050	2143	11.39	1/1/1981	7/25/1983	7/25/1983
106	1165.614	-800.839	2106	1905	12.45	1/1/1981	1/1/1983	1/1/1983
107	518.3775	-412.311	2150	1947	11.4	1/1/1981	1/1/1983	1/1/1983
108	1121.391	5.522499	2166	1964	12.17	9/1/1983	9/1/1985	9/1/1985
109	426.9886	-1245.69	2132	2044	11.57	7/1/1981	7/25/1983	7/25/1983
110	-153.281	-807.794	2140	1982	11.42	1/1/1981	1/1/1983	1/1/1983
111	1095.296	2266.909	2130	1998	11.21	1/1/1983	3/1/1984	3/1/1984
112	-241.881	-1550.89	2065	2040	10.98	12/2/1982	11/30/1984	11/30/1984
113	1066.019	-1562.79	2134	2066	7.07	1/1/1984	10/31/1985	10/31/1985
114	-856.484	-1799.09	2130	2036	8.23	8/1/1985	8/1/1987	8/1/1987
115	-1642.52	-1571.86	2146	1984	10.32	9/1/1984	8/1/1986	8/1/1986
116	-2359.92	-1338.53	2100	1845	10.74	8/1/1984	8/1/1986	8/1/1986
3	-2008.08	-701.695	1560	120	6.44	1/1/1946	1/1/1947	P&A

This capability also allows the generation of several pre-defined leach layers, or "onion-skin" layers, that represent the salt removed from a cavern during a drawdown process (when the oil in a cavern is removed with fresh water, which dissolves or leaches salt from the cavern wall). A typical rule-of-thumb (based on historical operations) is that the amount of salt removed from a cavern during a drawdown is about 15% of the volume of fresh water pumped into the cavern. Thus, the onion skins built into the mesh typically represent 15% progressive increases in the cavern volume along the entire height of the cavern. For this analysis, five leach layers have been constructed for each cavern except for caverns 2, 3, and 5 for operational reasons. Finally, the caverns and their leach layers have been constructed within a cylinder that fits into the holes in the mesh shown in the top part of Figure 9. These cylinders allow for block-specific designation of creep parameters for the purpose of trying to match historical cavern volume loss based on cavern pressure histories.

Figure 10 compares the old geometry for the BM Phase 2 caverns (red) built in 2017 and the recently updated geometry (yellow). Most of the caverns from new sonar data have the larger volume than one from the old sonar data due to dissolution of salt over time, while some caverns have the smaller volume potentially due to creep closure (e.g. BM112). The updated cavern geometries/mesh can lead to changes in stress states along the cavern wall as well as surrounding formation, so that following geomechanical analyses has been performed

A. Cavern volume calculation, which will be matched to the CAVEMAN data, to have new parameter values for MDV model
B. Estimate of stress-related damage potential by obtaining new minimum damage factors and maximum principal stresses for each cavern.

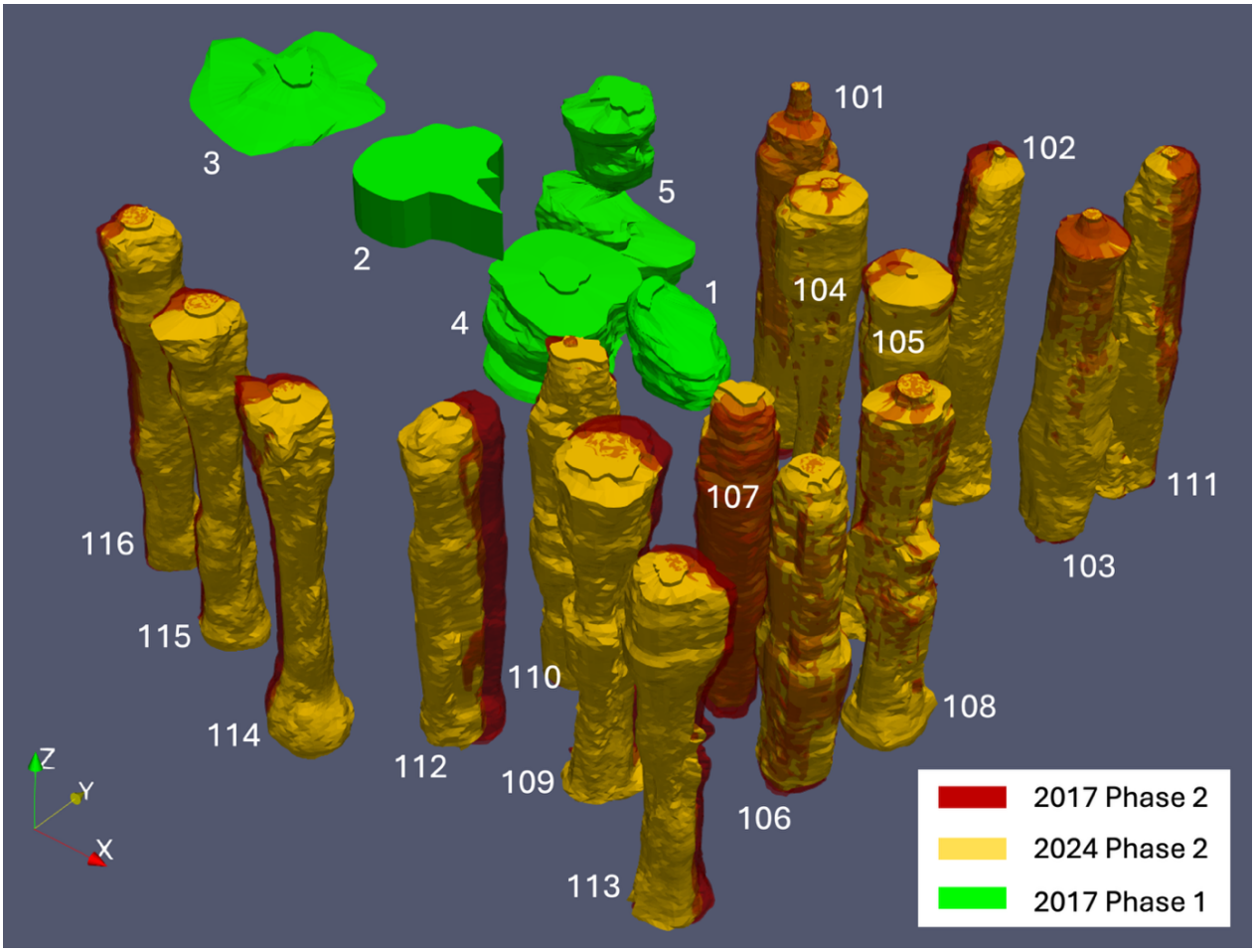

Figure 10. Bryan Mound caverns in a numerical domain. The red and green volumes represent BM cavern geometries built in 2017 while the yellow ones are for cavern geometries updated in 2024.

This report illustrates the recently updated geometry for BM105 as an example. The BM105 cavern was developed from two separate wells (B- and C-wells), which resulted in two separate caverns that were no smoothly joined initially into the single cavern shape we typically expect. The 2016-2017 computational geometry of BM105 was built based on sonars from C-well only, where the hidden portion of cavern wall between 2840 and 3600 ft depth due to shadowing was assumed to have uniformly cylindrical shape (red domain in Figure 11). Recent sonars from B-well provide information for the hidden portion, and thus, the new geometry generated by combining sonar data from B-well in 2023 and C-well in 2012 can provide a more realistic shape of entire BM105 (yellow domain in Figure 11) with smoother changes of the cavern wall in a vertical direction (e.g., eliminating an abrupt reduction of cavern perimeter at the hidden portion of 3500 ft depth). The vertical notches positive into the cavern are still present because the cavern has not been fully developed (Figures 11C and 11D).

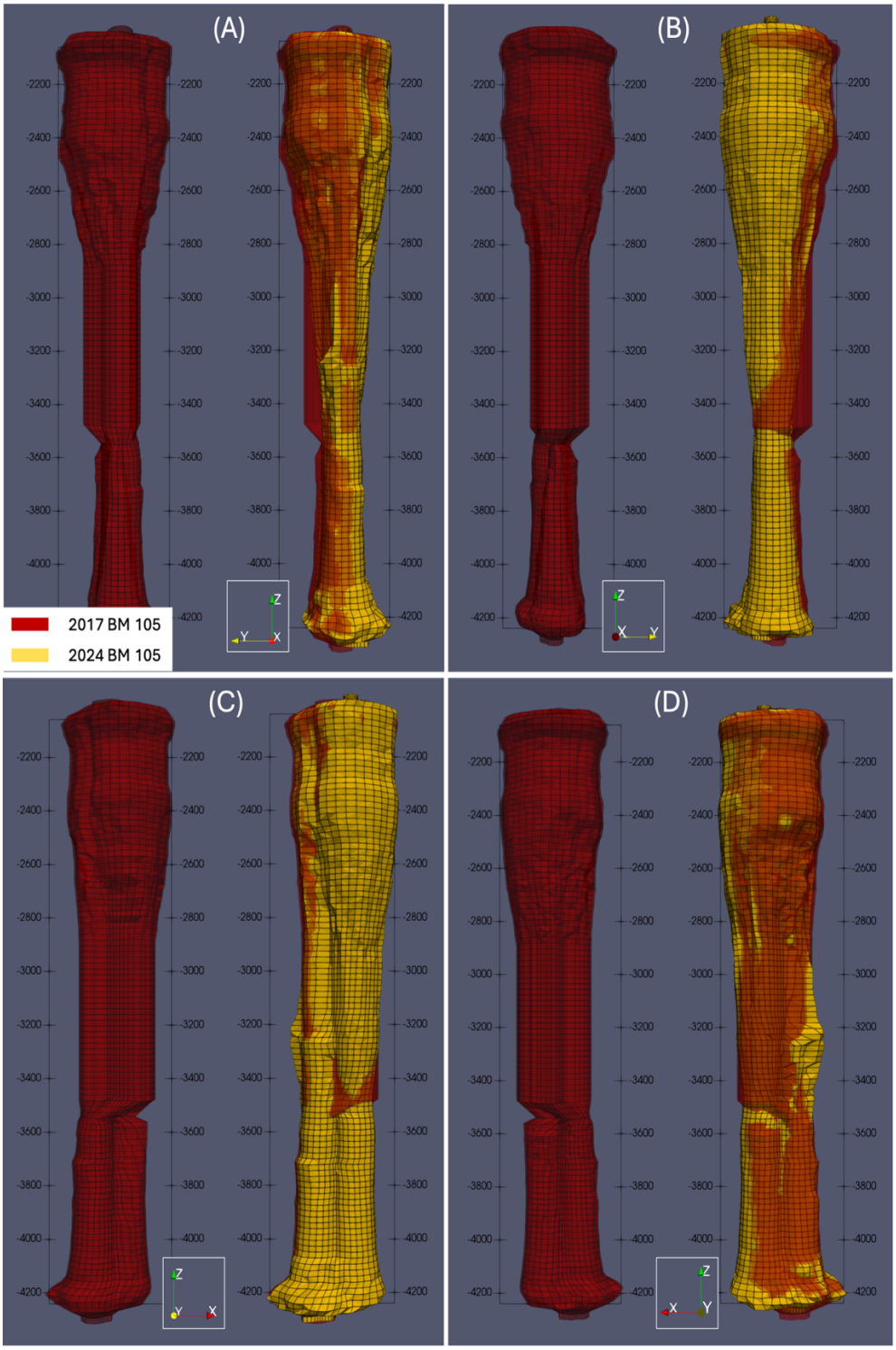

Figure 11. Comparison of old (2017; red) and new (2024 update; yellow) geometries of BM115 in four different directions. In each figure, the right-side plot shows duplicated geometries.

3.3. Computational and Material Models

3.3.1. Computational Model Setting

This analysis utilized the high-performance finite element code Adagio (Sierra Team, 2022), a three-dimensional finite element program developed by Sandia National Laboratories, and designed to solve large quasi-static nonlinear mechanics problems. Adagio is written for parallel computing environments, and its solvers allow for scalable solutions of very large problems. Adagio uses the SIERRA Framework, which allows for coupling with other SIERRA Mechanics codes. The development of the SIERRA Mechanics code suite has been funded by the Department of Energy (DOE) Advanced Simulation and Computing (ASC) program for nearly twenty years (Stewart and Edwards, 2003). The goal is development of massively parallel multi-physics capabilities to support the Sandia engineering sciences mission. SIERRA Mechanics was designed and developed from its inception to run on the latest, most sophisticated, massively parallel computing hardware. It has the capability to span the hardware range from a single workstation to computer systems with thousands of processors. The foundation of SIERRA Mechanics is the SIERRA toolkit, which provides finite element application-code services such as: (1) mesh and field data management, both parallel and distributed; (2) transfer operators for mapping field variables from one mechanics application to another; (3) a solution controller for code coupling; and (4) included third party libraries (e.g., solver libraries, communications package, etc.). The SIERRA Mechanics code suite comprises application codes that address specific physics regimes. Adagio is used for solid mechanics problems by solving quasi-static, large deformation, large strain behavior of nonlinear solids in three dimensions. Adagio has Sandia-developed (i.e., proprietary) technology for solving solid mechanics problems, that involves matrix-free iterative solution algorithms for efficient solution of extremely large and highly nonlinear problems. This advanced technology is especially well-suited for scalable implementation on massively parallel computers.

3.3.2. Salt Material Model Description

Plastic deformation of intact salt is isochoric and only occurs in the presence of shear stress. The original M-D model (Munson, 1998) considers three separate steady-state creep mechanisms and an overlying transient creep mechanism. Recent efforts by Reedlunn (2018) and others have resulted in some new understandings of steady-state creep, particularly at low stress states. This work has resulted in an upgrade to the original M-D creep (MDC) model in Adagio that is called the M-D Viscoplastic (MDV) model. The MDV model includes following changes made to the original MD creep model:

<u>Introduction of Hosford stress as the equivalent stress</u>
The formulation of Hosford stress is defined as follows:

$$\bar{\sigma} = \left\{\frac{1}{2}\left[|\sigma_1 - \sigma_2|^a + |\sigma_2 - \sigma_3|^a + |\sigma_3 - \sigma_1|^a\right]\right\}^{1/a}, \quad (1)$$

where σ_i are the principal stress components and a is a material parameter (different types of equivalent stress can be defined by the value of a). Eq. (1) encompasses the Tresca stress ($a = 1$ or 4), the von Misses stress ($a = 2$ or ∞), and a range of behaviors in-between.

<u>Addition of steady-state Mechanism 0</u>

The MDV model implements four mechanisms to describe the steady-state creep rate: (1) low-stress creep behavior ($i = 0$; Mechanism 0), (2) dislocation climb at high temperatures and low stresses ($i = 1$; Mechanism 1), (3) cross-slip ($i = 2$; Mechanism 2), and (4) dislocation glide ($i = 3$; Mechanism 3). These mechanisms can be expressed mathematically by

$$\dot{\bar{\epsilon}}^{ss} = \sum_{i=0}^{3} \dot{\bar{\epsilon}}_i^{ss}, \tag{2}$$

$$\dot{\bar{\epsilon}}_i^{ss} = A_i \exp\left(-\frac{Q_i}{RT}\right)\left(\frac{\bar{\sigma}}{\mu}\right)^{n_i} \qquad for\ i = 0, 1, and\ 2, \tag{3}$$

$$\dot{\bar{\epsilon}}_3^{ss} = H\left(\bar{\sigma} - \bar{\sigma}_g\right)\sum_{i=0}^{2} B_i exp\left(-\frac{Q_i}{RT}\right) sinh\left(q\frac{\bar{\sigma}-\bar{\sigma}_g}{\mu}\right) \qquad for\ i = 3, \tag{4}$$

where the variable A_i, B_i, Q_i, n_i, $\bar{\sigma}_g$, and q are model parameters. All for mechanisms have an Arrhenius temperature dependence, where Q_i is an activation energy and $R = 8.314$ [J/(K-mol)] is the universal gas constant. An actual micro-mechanical mechanism for the creep behavior at low equivalent stresses has not been identified yet, so the new mechanism, Mechanism 0, is simply given the same mathematical form as Mechanisms 1 and 2. Mechanism 1 is meant to capture dislocation climb, which dominates at high temperatures and low equivalent stresses. Mechanism 2 dominates at low temperatures and medium equivalent stresses. The micro-mechanical cause for mechanism 2 is also unknown, but cross-slip has been recently suggested (Hansen, 2014). Regardless, the macroscopic behavior corresponding to the second mechanism has been well characterized. Mechanism 3 models dislocation glide, which is only activated when $\bar{\sigma}$ exceeds $\bar{\sigma}_g$, as reflected in the Heaviside function in Eq. (4). Typically, the parameter B_i is chosen to produce a smooth transition to mechanism 3 at $\bar{\sigma}_g$.

Addition of transient strain limit Mechanism 0

The transient creep at low equivalent stress is captured by the following expression:

$$\dot{\epsilon}^{tr^*} = \sum_{i=0}^{1} \dot{\epsilon}_i^{tr^*}, \tag{5}$$

$$\dot{\epsilon}_i^{tr^*} = K_i \exp(c_i T)\left(\frac{\bar{\sigma}}{\mu}\right)^{m_i}, \tag{6}$$

where K_i, c_i, and m_i are parameters to be calibrated against experimental results. The new transient strain limit mechanism (Mechanism 0) is given the same mathematical form as the original mechanism. Note that notation of K_0 in the original MDC model is changed to K_1 because K_0 is used for Mechanism 0 in the MDV model.

To summarize, the MDV model includes the following changes to the original MDC model formulation:

1. The equivalent stress was generalized from Tresca to Hosford in Eq. (1)
2. Steady-state mechanism 0 was added in Eq. (3)
3. Transient strain limit mechanism 0 was added in Eq. (6).

3.4. Material Properties of Salt

It is desirable in large geomehcanical calculations to use salt properties that have been obtained through both laboratory experiments and through corroboration with measured field data such as cavern closure and surface subsidence. Laboratory values for SPR salts in Munson (1998) identify the West Hackberry and Big Hill salts as "soft" salts, and Bayou Choctaw and Bryan Mound as "hard" salts. For the Bryan Mound site, these properties were further calibrated by numerical analysis to match the estimated cavern closure and measured surface subsidence rates at the site (Sobolik and Ehgartner, 2009a, 2009b, 2012a & 2012b; Sobolik, 2010; Sobolik and Lord, 2014). The starting point for the property values for Bryan Mound were developed from laboratory tests on core reported in Munson (1998); that property set for the salt creep model is listed in Table 2. The development of the property sets used in the Sandia dome-scale model have advanced from the use of the power law creep model to the recent MDV model, from modeling overall properties for "hard" and "soft" sections of the Bryan Mound salt dome, and to estimation of "cavern-specific" creep properties in the regions immediately surrounding each cavern.

Table 2. Mechanical properties of salt for M-D Viscoplastic model.

Property	Bryan Mound salt properties
Density, lb/ft^3	144 (2300 kg/m^3)
Elastic modulus, lb/ft^2	648 $\times 10^6$ (31.0 GPa)
Shear modulus G, lb/ft^2	259 $\times 10^6$ (12.4 GPa)
Poisson's ratio	0.25
*Low-stress Creep Constant A_0, sec^{-1}	1
*Exponent n_0	1.6
Primary Creep Constant A_1, sec^{-1}	1.445 $\times 10^{22}$
Exponent n_1	5.5
Q_1, cal/mol	25000
Secondary Creep Constant A_2, sec^{-1}	1.667 $\times 10^{12}$
Exponent n_2	5.0
Q_2, cal/mol	10000
B_1, sec^{-1}	1.049×10^6
B_2, sec^{-1}	0.523×10^{-2}
σ_0, , lb/ft^2	429 $\times 10^3$ (20.57 MPa)
q	5335
m	3.0
K_0	6.275×10^5
c (1/R) (0.009198/1.8)	0.00511
α	-17.37
β	-7.738
δ	0.58

* The MDV model adds two parameters that describe salt creep behaviors at low stress states.

The necessity for developing improved M-D property sets for Bryan Mound is explained by the wide variability in the estimated cavern closure rates for each cavern. Table 3 lists the average cavern closure rates for each Bryan Mound cavern over three different time periods, which were used for the previous Bryan Mound model. Note that for the Phase 2 caverns (101-116) which have

similar geometries and depths, there is an order of magnitude difference in closure rates. These closure rates are derived from the wellhead pressure histories from each cavern, from which the code CAVEMAN (Ballard and Ehgartner, 2000; Ehgartner, 2004 & 2009) calculates a cumulative loss in cavern volume. The ultimate goal of the modeler is to develop a set of salt creep model properties, along with the given model, that produces predicted cavern volume loss, cavern deformation, and surface subsidence as close to estimated/measured values as possible. Previous Bryan Mound analyses cited above had greater success in matching measured surface subsidence than for estimated cavern volume loss. Because of the importance in understanding the effects of salt creep on the borehole casings in the salt, and on cavern integrity, it was decided to place greater priority on matching the cavern volume loss behavior in the simulations.

In this new Bryan Mound model, a series of different simulations was run with the computational mesh described herein, and with the known pressure histories through 1/29/2025, while varying the low-stress steady-state creep coefficient A_0 in addition to two specific property values of the secondary creep coefficient A_2 and the transient coefficient K_1 as done for the previous calibration based on the original MDC salt model.

Table 3. Cavern closure rates at Bryan Mound as determined from CAVEMAN.

	Cavern closure rates estimated from CAVEMAN, BBL/year		
Cavern	1/1/1990-7/26/2016	1/1/1990-12/31/2007	1/1/2008-7/26/2016
BM1	2622	2422	3041
BM2	284	274	307
BM4	11775	11390	12458
BM5	22275	25581	15298
BM101	9579	8918	10960
BM102	7616	6018	10960
BM103	17581	16508	19690
BM104	10304	10482	9888
BM105	6306	6943	4950
BM106	19635	18204	22602
BM107	12126	14168	7820
BM108	9235	10542	6437
BM109	15090	16064	13016
BM110	7753	7270	8241
BM111	9531	8259	12148
BM112	16105	14902	18482
BM113	16218	16253	16061
BM114	23479	25007	20249
BM115	25028	24943	25310
BM116	10370	10417	10249

The low-stress steady-state creep coefficent A_0 represents the impact of low-stress creep mechanism on the cavern closure, but the reference value of A_0 ($A_0 = 1$) is arbitrarily chosen due to absence of experimental data from creep tests on salt samples. The creep coefficient A_2 was chosen because that creep mechanism is the dominant steady-state creep mechanism. The transient coefficient K_1 was chosen to capture the large volume change that occurs during a workover.

Comparison of the cavern volume changes from the Sierra simulation to the CAVEMAN data provides the ratio of a new value of three coefficients to the reference value given in Table 2 that defines "multipliers" to vary the cavern-specific creep properties. Note that all other values listed in Table 2 were unchanged. Because of the large amount of time to run a simulation through the existing life of the facility, only seven such simulations were performed to optimize the mulitplier values.

The set of multipliers that produced the best agreement with the estimated cavern volume closure data are listed in Table 4. The MDV creep properties represented by these values were used to obtain the results presented throughout this report. For most of the caverns, the same set of properties were used for the six skin layers that surround the cavern and the cylinder that surrounds those skin layers. However, for a few caverns the cylinder was given different properties, to balance out the effect of workovers from one cavern affecting closure in adjacent caverns The results shown in Section 4 will depict a better agreement with the CAVEMAN derived data, but at a cost of the overprediction of surface subsidence. An updated verification of the methodology CAVEMAN uses to calculate cumulative cavern volume change from wellhead pressure data will be performed in the near future, and this will give better insight into the appropriateness of the coefficient multipliers in Table 4 used for these analyses.

Table 4. Multpliers applied to Low-stress Creep Coefficient A_0, Secondary Creep Coefficient A_2, Transient Coefficient K_1 for each dome or cavern region, for analyses in this report.

Salt of Cavern Region	A_0 multiplier	A_2 multiplier	K_1 multiplier	Cylinder
Hard salt	1.0	2.3	1.0	--
Soft salt	10.0	24.0	1.0	--
BM1 (leach layers + cylinder)	1.0	6.0	1.0	Same
BM2 (leach layers + cylinder)	1.0	19.08	1.0	Same
BM3 (leach layers + cylinder)	1.0	19.08	1.0	Same
BM4 (leach layers + cylinder)	1.0	31.0	1.0	Same
BM5 (leach layers + cylinder)	1.0	1.94	1.0	Same
BM101 (leach layers + cylinder)	0.95	1.89	0.1	Same
BM102 (leach layers + cylinder)	0.15	5.0	0.1	Same
BM103 (leach layers + cylinder)	0.01	50.0	0.5	Same
BM104 (leach layers + cylinder)	12.5	1.46	2.0	Hard salt
BM105 (leach layers + cylinder)	0.001	1.85	1.0	Same
BM106 (leach layers + cylinder)	0.9	25.	1.0	Same
BM107 (leach layers + cylinder)	1.2	1.5	1.0	Hard salt
BM108 (leach layers + cylinder)	0.001	0.14	1.5	Hard salt
BM109 (leach layers + cylinder)	0.9	7.0	1.0	Same
BM110 (leach layers + cylinder)	0.005	1.5	1.0	Same
BM111 (leach layers + cylinder)	1.05	20.0	0.16	Same
BM112 (leach layers + cylinder)	10	1.5	1.5	BM109
BM113 (leach layers + cylinder)	0.01	40.0	1.0	Soft salt
BM114 (leach layers + cylinder)	0.01	200.0	1.0	Soft salt
BM115 (leach layers + cylinder)	0.85	200.0	1.0	Soft salt
BM116 (leach layers + cylinder)	0.9	4.36	1.0	Same

3.5. Other Material Properties

The surface overburden layer, which mostly comprises sand and sandstone, is considered isotropic and elastic, and has no assumed failure criteria. The caprock layer, consisting of anhydrite and limestone with some gypsum, is also assumed to be elastic for this analysis. As described earlier, several well casing failures at the Bryan Mound site indicate that the caprock has been significantly altered due to steam-injection sulfur mining from the early 1900s, which both compromised the mechanical integrity of the caprock and left a significant increase in temperature that still remains. The caprock was also known to be significantly rubblized in various locations. Therefore, the caprock does not behave in a homogeneous, elastic manner in its entirety. For this analysis, though, it is modeled as an elastic medium to allow for an easier comparison with previous analyses, and to determine the potential effect of subsidence over Cavern 3 may have on the site. The sandstone surrounding the salt dome is assumed to be elastic (Lama and Vutukuri, 1978). Mechanical properties of each of these geologic materials used in the present analysis are listed in Table 5.

Table 5. Material properties of other geologic materials.

Parameters	Units	Overburden	Caprock	Sandstone
Density	lbm/ft^3	117.	156.	133.6
Young's Modulus	lb/ft^2	2.09×10^6	146×10^6	153×10^6
Poisson's Ratio		0.33	0.29	0.33

The sulfur mining in the caprock at Bryan Mound in the early 20th century was performed using the Frasch extraction method, for which superheated steam at 320°F was injected into the caprock to draw out sulfur, in a mostly molten form with some SO_2 and H_2SO_4. This steam remained in situ within the caprock, and the heat was contained in the caprock and conducted into the underlying salt dome. Borehole temperature logs were taken for each cavern between 2001 and 2003. These vertical temperature profiles are plotted in Figure 12. The caverns with the lowest maximum temperatures, Caverns 111, 114, 115, and 116, all lie on the periphery of the cavern field. The red linear plot in Figure 12 represents an in-situ profile based on an independent borehole temperature log in salt at cavern depth; this linear profile has been used in the past for modeling exercises. However, a curve fit based on the average measured temperatures was used for this analysis; this curve fit is also shown in Figure 12. Cavern 3 is located at depths between 1560 and 1680 feet, which puts it in a region where the measured borehole temperature is a few degrees higher than the linear in situ salt temperature. The salt above the cavern at the salt-caprock interface may be at temperatures 30°F higher than the in-situ temperature. The curve fit temperature profile for caverns located below 2000 feet of depth is nearly identical to the in situ linear equation used for Sobolik and Ehgartner (2009a & 2009b), so the different temperature profile is expected to have a negligible effect on predicted cavern closures and surface subsidence for those caverns. The curve fit temperature profile used for Bryan Mound is described by the following equations:

For depth z between 0 and 360 feet, $T = 72 + 0.09647z$
For depth z between 360 and 1040 feet, $T = -2.478E\text{-}4z^2 + 0.3857z$
For depth z between 1040 and 2000 feet, $T = -3.387E\text{-}5z^2 - 0.1179z + 219.05$
For depth z greater than 2000 feet, $T = 118.7 + 0.0153*(z-2000)$

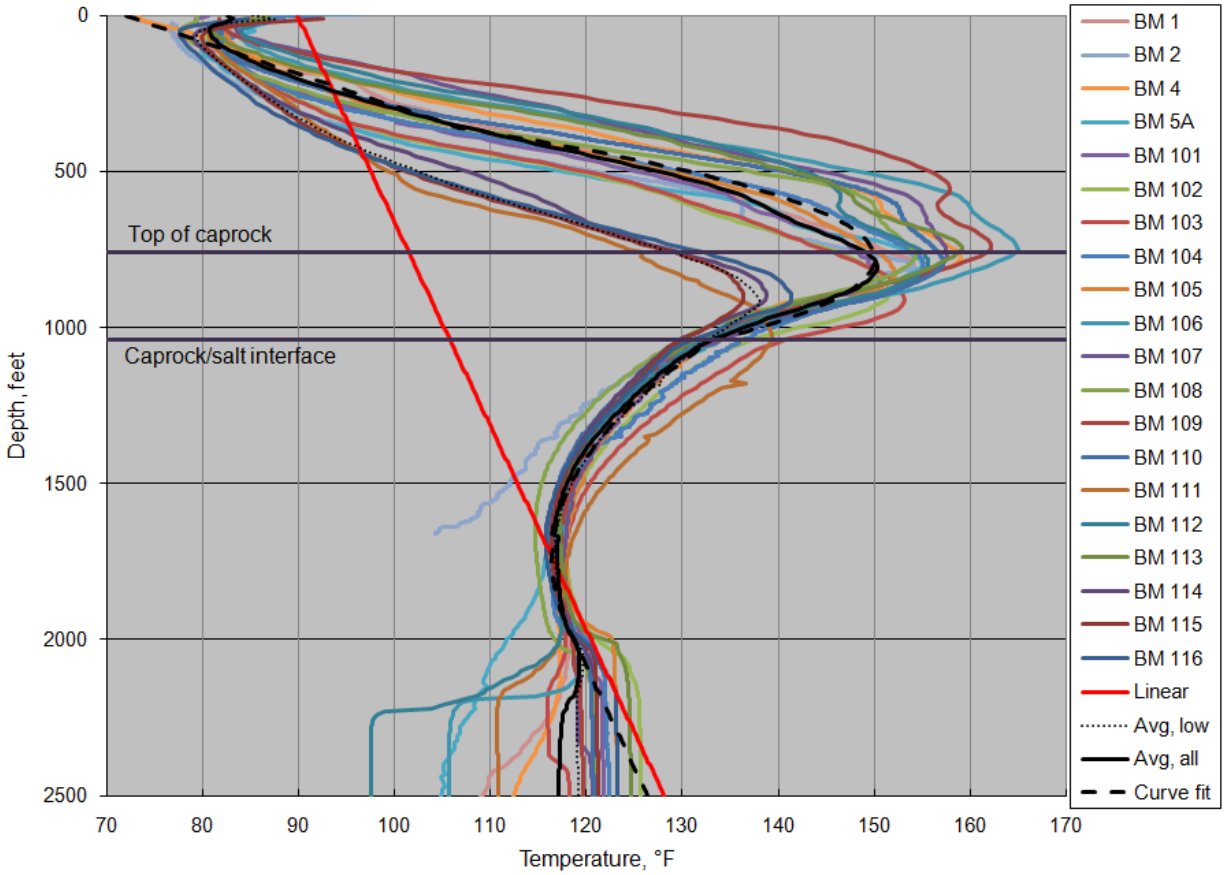

Figure 12. Bryan Mound temperature profiles, including measurements from each borehole, average values and curve fits.

3.6. Damage Criteria

The damage factor criterion (analogous to a safety factor) has been developed as a linear function of the onset of dilatant damage as a function of the hydrostatic pressure (Van Sambeek et al., 1993). Dilatancy is considered the onset of damage to rock resulting in increases in permeability. Dilatant damage in salt typically occurs at the stress state at which a rock begins microfracturing, causing an increase in the rock volume. Dilatant criteria typically relate two stress invariants: the mean stress invariant I_1 (equal to three times the mean stress) and the square root of the stress deviator invariant J_2, or $\sqrt{J_2}$ (a measure of the overall deviatoric or dilatant shear stress). (By convention, tensile normal stresses are positive, and compressive normal stresses are negative, hence the sign nomenclature in the following equations.) The dilatant criterion chosen here is the equation typically used from Van Sambeek et al. (1993),

$$\sqrt{J_2} = -0.27 I_1 . \qquad (7)$$

The damage criterion defines a linear relationship between I_1 and $\sqrt{J_2}$, and such a linear relationship has been established from many suites of laboratory tests on WIPP, SPR, and other salt

samples. This criterion was applied during post-processing of the analyses, using predicted stress states. A damage factor (safety factor) index was created (*SF*) by normalizing I_1 by the given criterion:

$$SF_{VS} = \frac{-0.27 I_1}{\sqrt{J_2}} \tag{8}$$

Several earlier publications define that the damage factor *SF* indicates damage when *SF*<1, and failure when *SF*<0.6. In previous studies, values of *SF*<1.5 have been categorized as cautionary due to unknown localized heterogeneities in the salt that cannot be captured in these finite element calculations. This report will use these damage thresholds.

In addition to the damage criterion based on deviatoric stresses, the onset of tensile stresses is also used as an indicator of fracture formation in the salt. Salt, like most geomaterials, has a very low tensile strength. Engineering literature spanning several decades list tensile strength values of salt ranging from 1 MPa to 3 MPa. For the purposes of this report, a value of 1 MPa (145 psi, or 20,900 psf) will be assumed.

4. RESULTS

The historical and predicted future performance of the Bryan Mound caverns was evaluated on the following four geomechanical factors: (1) creep-driven cavern volume closure, (2) axial strain in the caprock and salt, (3) dilatant and tensile stress damage to the salt surrounding the caverns, and (4) surface subsidence. In the first section, the geomechanical simulation results during the historical operations period will be compared to Bryan Mound data for cavern volume closure from CAVEMAN, to evaluate the effectiveness of the chosen salt material property sets. The second section will examine the predicted axial strains along the caprock and salt above the cavern top to evaluate the impact of caprock damage on the wellbore integrity, and the potential mechanism will be discussed. In the following section, the stress-related damage potential will be calculated by using damage criteria (refer to Section 3.6) based on spatio-temporal development of stresses in the salt surrounding the caverns. The discussion of tension and dilatancy will also be used to briefly describe how these analyses are used to determine the number of available drawdowns for each cavern.

When examining the results described in the following sections, it is important to remember that these calculations were performed with a specific set of assumptions. Even though the computational model has several options built into it to examine various geomechanical aspects of the Bryan Mound site, a single 80-year simulation takes 4-6 weeks to run even on high performance computing machines. Therefore, this analysis considers one set of assumptions; other assumptions will be considered in future model applications. The primary assumptions for this set of calculations include:

- The use of CAVEMAN-generated cavern volume closure (Ballard and Ehgartner, 2000) corresponding to historical wellhead pressures; there has been some recent discussions about the accuracy of the calculated volume changes, and a future task will reevaluate, revalidate, and probably reprogram the CAVEMAN algorithm to produce values more in line with recorded fluid exchanges in the caverns.
- The damaged caprock region is represented by variation in the caprock mechanical property. It was shown in previous Bryan Mound analyses (Sobolik, 2010) that a damaged caprock can have significant effects on the distribution of shear and normal stresses throughout the caprock, as undamaged sections of caprock will take on greater loads to compensate for the weakened mined areas. Note that the reference model assigns the same material model and properties to undamaged and damaged caprock regions because of the length of computation time for a full model run.
- These analyses were performed assuming that Cavern 2 would still be used as an oil storage cavern. During the time the calculations were run, the decision was made to fill Cavern 2 with brine and decommission its use for oil storage. The model was kept as is, and its results should still be useful for projecting the cavern's future behavior.

4.1. Calibration of MDV Model Parameter Values

The volume of the caverns decreases as the salts creeps. The only active measurements of cavern volume occur during sonar measurements of the caverns, and these are performed once every few years. The daily evolution of cavern volume change must be derived from knowledge about the creep rate of the salt under its given stress and temperature conditions, the compressibility of the fluid, and fluid pressure at any point in the cavern, which is a function of the pressure at the wellhead. The program CAVEMAN (Ballard and Ehgartner, 2000; Ehgartner, 2004 & 2009) is used

to calculate the daily change to cavern volume, based on the parameters previously stated. These values are not true measurments, but will be referred to as measured data throughout this report.

The MDV model adds the following changes to the original MDC (Multi-mechanism Deformation Creep) model (refer to Section 3.3 for more details):

1) Introduction of new definition of the equivalent stress using Hosford stress to describe plastic yielding, instead of Tresca stress used in the original MDC model. Note that the equivalent stress combines 9 stress vector components into a single scalar value to describe the total stress acting on the body of interest.
2) Addition of steady-state low-stress mechanism (steady-state mechanism 0)
3) Addition of transient strain limit mechanism at low equivalent stress (transient strain limit mechanism 0).

The addition of both steady-state and transient strain limit low-stress mechanisms will affect the geomechanical behavior of the salt rock. The cavern volume loss behavior can be an efficient indicator to verify the impact of low-stress mechanisms on the salt creep behavior because the cavern volume perturbs corresponding to the initial cavity volume and pressure history.

Figure 13 shows the temporal perturbation in the cavern volume for each Bryan Mound cavern predicted from Sierra/SolidMechanics simulation with MDC model (dashed lines) and MDV model (solid lines), respectively. Note that the low-stress creep parameter A_0 is not calibrated in this simulation run. The step changes correspond to workovers when the wellhead pressure was lowered to near zero; these times induce the greatest change in cavern volume as the differential stress in the salt is greatest and the strain rate due to creep is correspondingly highest. The difference between two lines indicates the impact of low-stress mechanisms on the salt creep rate. In general, the MDV model (solid lines) accelerates the cavern volume reduction over time mainly because of low-stress mechanisms (e.g., for BM101, the cavern volume decreases by about 2×10^6 [ft^3] in 2020 more when the MDV model is used; indicated by a red arrow in Figure 13). This result indicates that neglecting low-stress mechanisms, as done for previous geomechanical analyses with the original MDC model, may underestimate the cavern volume loss over time. The Phase 1 caverns (BM1, 2, 4 and 5) experience less impact of the low-stress mechanism (and also less cavern closure) because they are shallower than the other caverns, thus the lower stress differential between cavern pressure and in situ stress experienced.

In general, the predicted behavior of the caverns matches the measured behavior farily well, particularly the rates of volume change during the normal operations phases. The instances where large discrepancies occur tend to during the workovers, and also very early in the time period plotted. The comparisons shown here are significantly better than those published in earlier Bryan Mound studies, particularly Sobolik and Ehgartner (2009a). The reasons for the closer predictions include better cavern-specific creep coefficients, and the use of the actual cavern wellhead pressure histores. The caverns in the soft salt, primarily 114, 115, 113, and 106, have the highest average cavern closure rates, ranging from 0.15 to 0.23%/year, as shown in Figure 13. Caverns 1, 2, and 5 experience the least closure because they are shallower than the other caverns, thus avoiding the higher stress differential between cavern pressure and in situ stress experienced at greater depths. The maximum average closure rate for these caverns is 0.04%/year. In the hard salt, Cavern 103 has the highest average closure rate at about 0.13%/year. The site average closure rate for Bryan Mound

is 0.096%/year. This point substantiates the notion that, on average, Bryan Mound is a harder salt, even though it has significant localized heterogeneities. For all the cylinderically-shaped caverns, the majority of the volume loss occurs near the bottom of these caverns because of the greater stress differential at lower depths.

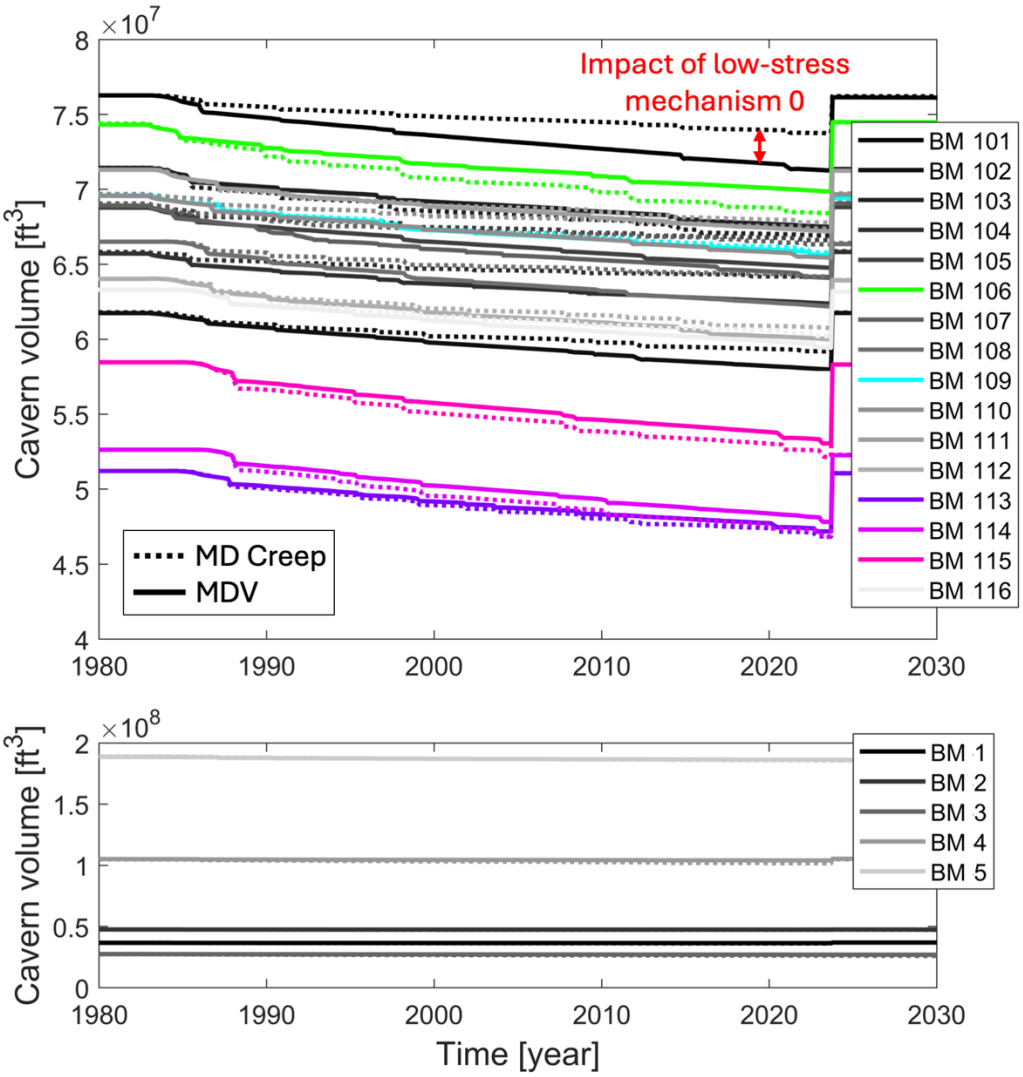

Figure 13. Temporal evolution of cavern volumes. Dashed and solid lines represent results from MD creep and MDV models, respectively. Colored lines are for the caverns within a soft salt.

Note that the current MDV model uses the parameter values calibrated against the experimental data measured from the WIPP (Waste Isolate Pilot Project) bedded salt, not the Bryan Mound domal salt, such that the MDV model with additional low-stress mechanisms may not capture the creep behavior of the Bryan Mound salt properly. To minimize this uncertainty driven by the limited database for the BM salt, an additional process of validating the MDV model by matching the predicted cavern volume changes to the CAVEMAN data. The CAVEMAN program calculates the daily changes to cavern volumes based on wellhead pressures, fluid temperatures, the depth of the oil/brine interface, and the cavern geometry. The volume of the caverns decreases as the salts

creeps. The only active measurements of cavern volume occur during sonar measurements of the caverns, and these are performed once every few years. The daily evolution of cavern volume change must be derived from knowledge about the creep rate of the salt under its given stress and temperature conditions, the compressibility of the fluid, and fluid pressure at any point in the cavern, which is a function of the pressure at the wellhead. This calibration process enables to obtain the reasonable value of cavern-specific "multiplier" for the MDV model parameter, especially for the low-stress creep mechanism, for the Bryan Mound geomechanical analysis.

To obtain the values for "multipliers" for the MDV model parameter, a series of sensitivity tests with variation in the structure factor of "steady-state Mechanism 0" ($A_0 \equiv$ steady-state creep parameter at a low equivalent stress condition given in Eq. (2); Section 3.3) are performed within the reasonable range of A_0 for the domal salt to examine the effect of changing A_0 on cavern volumetric closure. The smaller A_0 will result in less impacts of the additional low-stress steady-state creep mechanism on the cavern closure. For the properties for the other standard MD components of the model, the properties for Bryan Mound MDC model developed in Munson et al. (1998) were used for all the caverns with multipliers applied to secondary steady-state creep coefficient A_2 and transient coefficient K_1 (K_0 in the original MDC model) as done in previous geomechanical model analyses (e.g., Sobolik, 2018). This report illustrates the process of the MDV model parameter calibration for the cavern BM105 as an example.

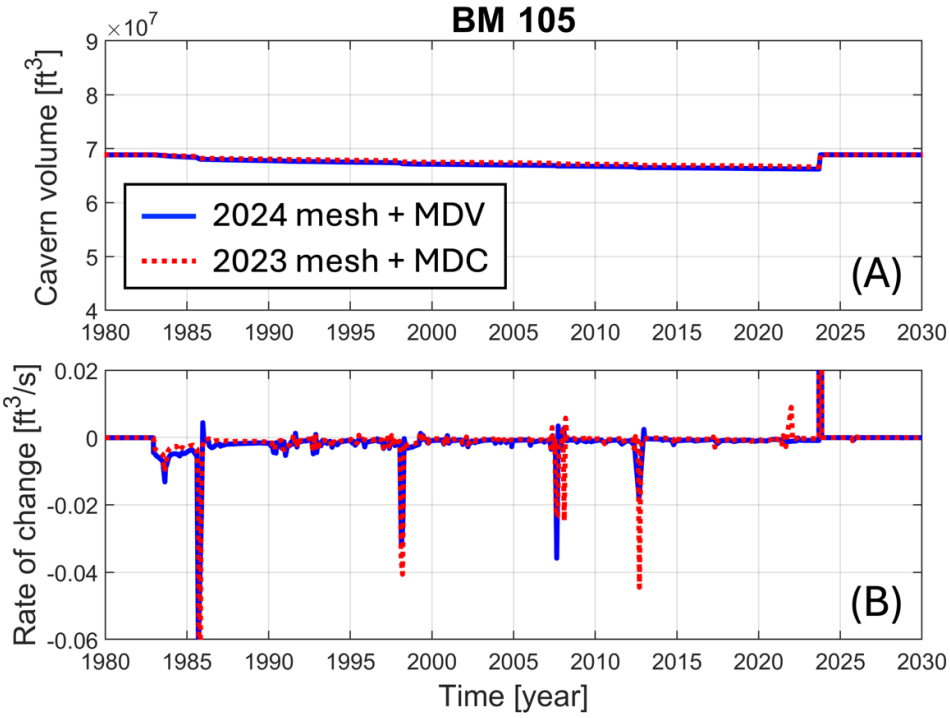

Figure 14. Comparison of cavern volume and rate of volume change over time from the MD creep (MDC) model (red dashed lines) and MD viscoplastic (MDV) model (blue solid lines) for BM105.

Figure 14 plots comparisons of the predicted cavern volume closure history and rate of cavern volume change from the MDC model (red dashed lines) and MDV moel (blue solid lines) for BM105. In general, the predicted behavior of the caverns from both salt models matches the

measured behavior farily well, particularly the rates of volume change during the normal operations phases with the following parameter values.

Table 6. Parameter values of the salt constitutive models for BM105.

Creep Mechanism	Parameter	Multiplier	
		MDC	MDV
Steady-state mechanism 0	A_0	N/A*	0.001
Steady-state mechanism 2	A_2	1.85	1.85
Transient mechanism 1	K_1 (K_0)†	1	1

*MDC doesn't include the low-stress mechanism, so that no A_0 value is defined.
†MDC model in the Sierra/SM software defines K_0 for the transient creep parameter.

The step changes in the cavern volume closure correspond to workovers when the wellhead pressure was lowered to near zero; these times induce the greatest change in cavern volume (spikes in the rate of volume changes shown in Figure 14B) as the differential stress in the salt is greatest and the strain rate due to creep is correspondingly highest.

4.2. Caprock Integrity Analysis

This letter summarizes the recent computational study of sensitivity tests to investigate how the variation in mechanical property of the caprock above the Bryan Mound salt dome and the cavern operation, potentially impacts the wellbore integrity. The simulation results support a potential physical mechanism of caprock deformation induced by damage that may provide insight as to the cause of the recent wellbore failure above the cavern 116 (well BM-116A).

4.2.1. Damaged Caprock Model

The caprock at Bryan Mound impacts stresses, strains and damage modes of the wellbore casings by the following parameters:

- The inelastic behavior of the caprock (e.g. deformation of void space)
- Mechanically weakened caprock caused by the sulfur mining with fracturing and steam-injection
- Thermal expansion and/or corrosive environment driven by latent heat (15-20°C higher than the ambient temperature) and/or elevated exposure of acids

This study reduces the Young's modulus by a factor of 10 arbitrarily to account for the creation of additional void space that can make the caprock easily compressed by loadings. Two different scenarios are tested; (1) scenario 1: only the unmined caprock region has a reduced Young's modulus and so becomes easily compressible and (2) scenario 2: the entire caprock is weakened by reduction in the Young's modulus (refer to Table 6). Note that no information on mechanical properties for the Bryan Mound caprock is available, so cited properties for caprock from the Big Hill geomechanical model are used (Park et al., 2006). The physical presence of well casings is not included in this model, but the potential for rock deformation that may damage these structures can be conservatively estimated by assuming that they will deform according to the predicted stresses and strains in the host rock.

Table 7. Model setting for sensitivity tests of caprock damage impact.

Description of model setting		Young's modulus [lb/ft^2]	
		Unmined caprock	Mined caprock
Reference	Both unmined and mined caprock regions have the same Young's modulus	14.6×10^7	14.6×10^7
Scenario 1	10 times less Young's modulus applied to the unmined caprock (upper light gray region) only	14.6×10^6	14.6×10^7
Scenario 2	10 times less Young's modulus applied to both caprock regions	14.6×10^6	14.6×10^6

- Less Young's modulus represents that the caprock becomes more compressible. Note that the compressibility is numerically equal to reciprocal of Young's modulus.
- BM116 wellbore assumes to be drilled though the unmined caprock.
- The reference value for the caprock Young's modulus is from the Big Hill model due to the absence of the material property information for the Bryan Mound caprock.

4.2.2. Geomechanical Model Results

The caprock damage can impact the distribution of normal and shear stresses throughout the whole caprock, as undamaged sections of caprock will take on greater loads to compensate for the weakened mined areas (Sobolik, 2010).

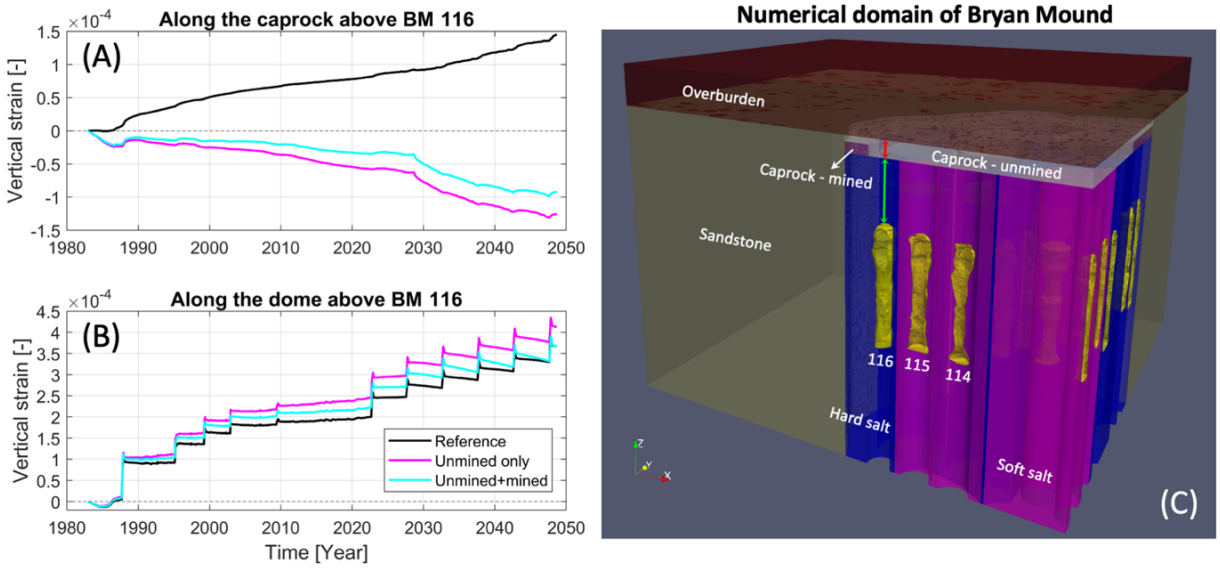

Figure 15. Model results of vertical strain (A) along the caprock above BM116 from -760 to -1400 ft of depth (red line in Figure 15C) and (B) along the dome from -1400 to -2000 ft of depth above BM116 (green line in Figure 15C). Temporal changes of vertical strains are obtained from three scenarios: (1) reference model used for the Bryan Mound geomechanical analysis (black lines), (2) only unmined caprock is weakened (magenta lines), and (3) both unmined and mined caprocks are weakened (cyan lines).

The impact of caprock damage is quantified by the axial strains in the caprock and salt dome above the top of BM116 (Figures 15A and 15B) along the vertical lines from the depth of -760 ft (caprock top) to -1040 ft (interface between caprock and dome) and from the depth of -1040 ft to -2140 ft (cavern top), indicated by red and green lines, respectively (Figure 15C). Normal strain occurs when the elongation of the object is in response to a normal stress. A positive value corresponds to a tensile strain, while negative is compressive.

The result shows that the presence of damaged caprock leads to a negative stain within the caprock (Figure 15A) and a positive strain within the dome (Figure 15B). This implies that the caprock is squeezed in a vertical direction resulting from the expansion of the pressurized cavern and dome above the operating cavern. This geomechanical simulation result is consistent with the field observation of wellbore failure within a caprock region above BM116, potentially driven by compression in a vertical direction.

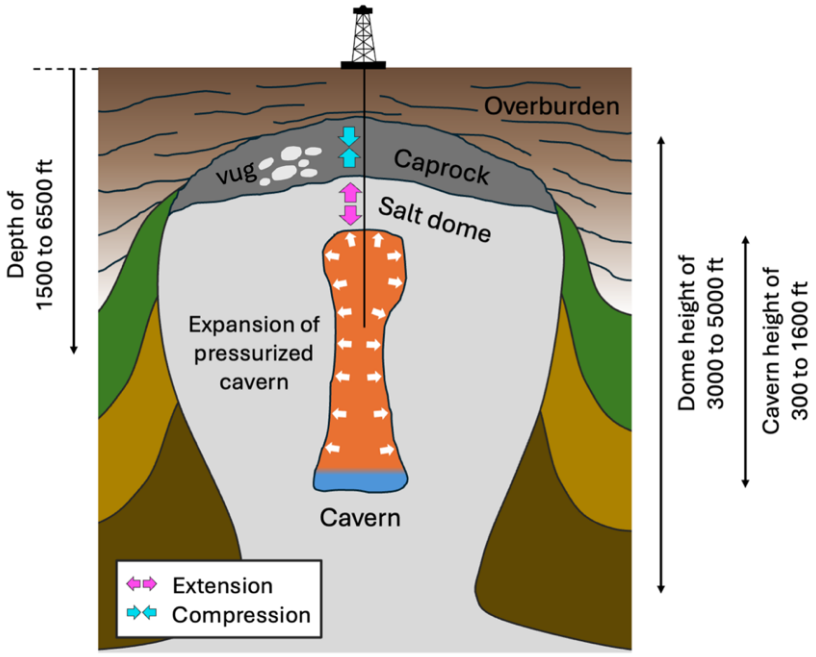

Figure 16. Schematic description of physical mechanism for the geomechanical behavior of the cavern and surrounding formations under the presence of more compressible, potentially resulting from caprock damage.

Figure 16 describes schematically how the caprock damage impacts the geomechanical behavior of the operating cavern and surrounding formations. The presence of vugs or fractures introduces more compressible elements, such as air or fluids, into the caprock, which can deform under pressure, leading to a larger overall volume change for a given applied pressure. Geomechanically, more compressible caprock becomes easier to compress by the instantaneous relative change in a rock volume as response to the increase in the mean stress. Hence, the expansion of a pressurized cavern, resulting from oil storage and/or salt creep, generates axial extension in a salt dome directly above the cavern. On the other hand, the caprock experiences axial compression because the damaged caprock is squeezed (compressed) more easily under the same amount of compressive load.

The case in which the whole caprock becomes more compressible gives smaller vertical strains within the caprock and salt dome (cyan lines in Figures 15A and 15B) because more volumes of caprock are compressed under the same change in the means stress that mitigates the vertical deformation of both caprock and dome. This result suggests that the partial damage of the caprock will localize the stress perturbation, such that the stress concentration, a localized area of high stress, may induce substantial deformation compared to other areas.

4.3. Stress-related Damage

Lower values for dilatant damage factor indicate a higher likelihood for dilatant damage, with values <1.5 considered cautionary, values <1.0 indicating the onset of damage, and values <0.6 indicating failure of the salt, primarily in the form of substantial increase in permeability due to microcracking. In the computational mesh used for these analyses, each cavern is surrounded by a cylinder of salt. The vast majority of the salt in each of the cylinders exists at very low deviatoric stress value, and thus very high values for the damage factor; only in the cavern walls and near vicinity are there sufficient deviatoric stresses to lower the damage factor significantly. The other indicator of salt damage is the maximum principal stress. Salt fractures under very low tensile stress (on the order of 1 MPa or 145 psi), so any indication of tension in the salt is of concern.

In general, the location of the predicted lowest value for damage factor and/or positive maximum principal stress occurs in one of three places in the cavern: (1) the ceiling, where the cavern pressure is much less than the in situ pressure in the salt; (2) the base of the cavern, which can either occur at a cavern "foot" extending around the base of the cavern due to leaching, or an unusual geometry due to the sonar mapping process; and (3) stress concentrations in the side of the cavern due to protuberances wither into or out from the cavern. The downward spikes in temporal plots of the dilatant damage factor and/or upward spikes in maximum principal stress coincide with actual or projected workovers in that cavern, when the wellhead pressure is dropped to zero causing a commensurate drop in cavern pressure. These points in the history plots almost always occur in the ceiling, so it is during these times that salt falls are more likely to occur. However, workover-induced salt falls are by themselves a strong indicator of cavern integrity issues, although they have significant potential to damage hanging strings and cause operational issues. It is more important to examine these plots for significant operational periods for which some region of the cavern wall may be experiencing dilatant stresses, when damage factors are less than 1.0 and/or tensile stress under the positive maximum principal stress state.

This report shows the potential of stress-related damage on the cavern wall only for the caverns experience the dilatant damage factor less than 1 and/or maximum principal stress larger than 0 from the geomechanical simulations, which are BM105, 108 and 109.

4.3.1. BM105

Figures 17A and 17B show the minimum value of the damage factor and maximum value of the maximum principal stress at any point around the cavern BM105, respectively, as a function of time through five drawdowns. Two model results are compared; one from an old model with MDC salt model (dashed lines) and another from a new model updated with a new cavern geometry based on recent sonar data, MDV salt model, and a new cavern pressure history (solid lines).

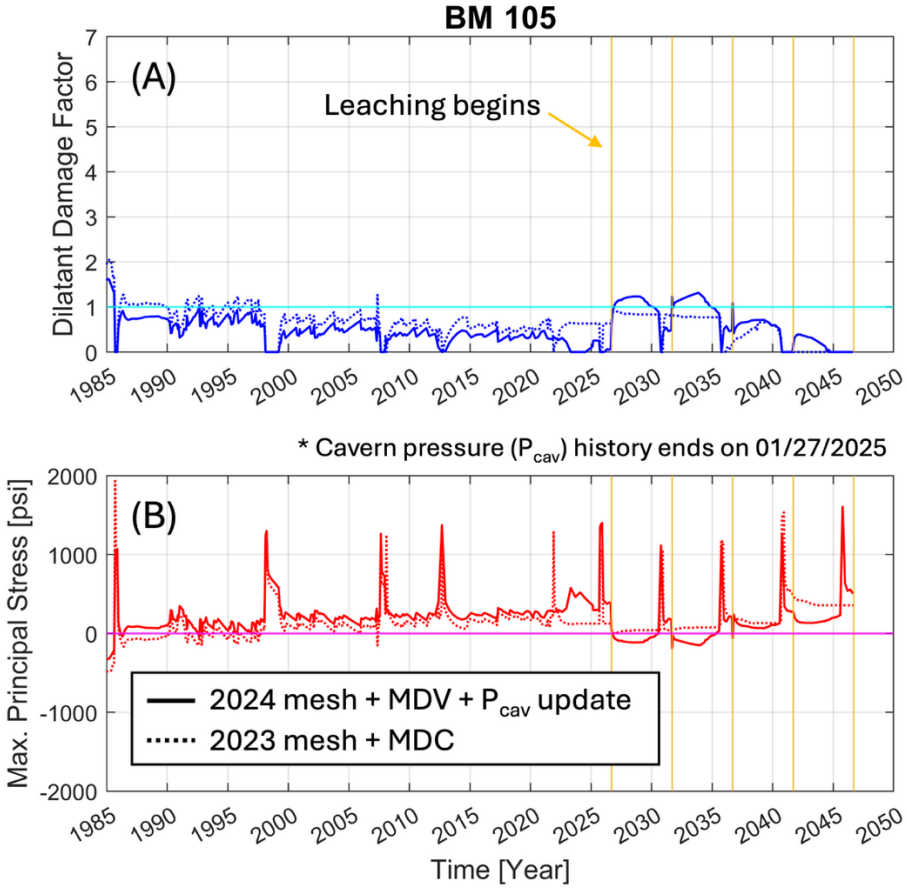

Figure 17. Stress-related damage analysis of BM105. (A) Predicted minimum damage factor for BM105 and (B) maximum principal stress in salt surrounding BM105. The dashed lines are for MDC model results, while solid lines are for MDV model results.

Figure 17A shows the minimum value of the damage factor surrounding BM105 as a function of time. The low values of damage factor less than 1 are observed after the 2nd leaching operation, which implies that stress concentrations would be expected within the salt surrounding the cavern. Also, the new model predicts that absolute values of dilatant damage factor become less than what were observed from the old model (solid line in Figure 17A). This result suggests that the update of model setting, implementing a recent cavern geometry and low-stress creep mechanism, may increase the potential of shearing-induced failure.

The maximum normal stress is determined from the maximum principal stress at each location in the salt; positive values indicate tension, and negative values are compressive stresses. Much as for the damage factor, the spikes in the histories for each cavern usually represent times when that cavern is undergoing a workover (smaller "sub-spikes" are often one cavern's response to a neighboring cavern undergoing a workover). For the majority of the caverns, the maximum normal stress is comfortably in the compressive regime except during workovers, when typically, an area in the cavern may experience momentary tensile stresses. Figure 17B indicates that BM105 experiences

significant periods of time during their histories when some portion of the cavern exhibits tensile stress behavior.

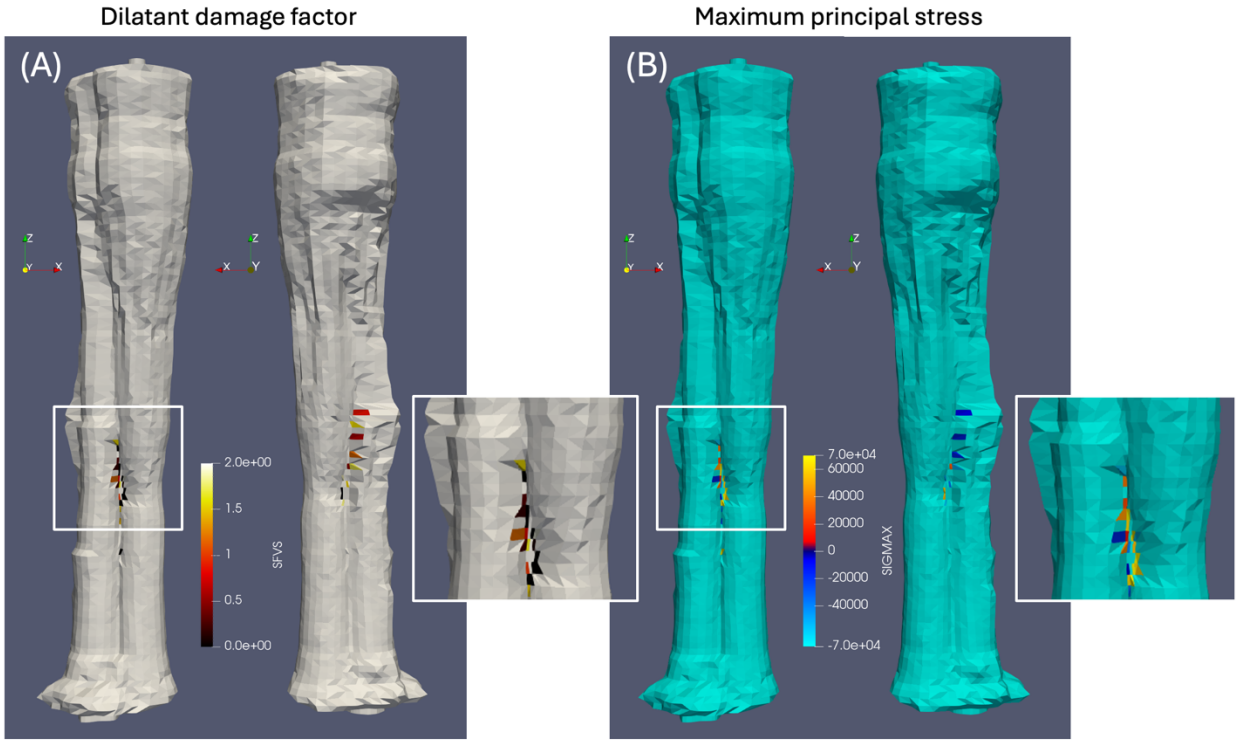

Figure 18. Three-dimensional distribution of (A) dilatant damage factor and (B) maximum principal stress on the BM105 cavern wall at the end of simulation run (August 12, 2051).

The spatial distribution of dilatant damage factor and maximum principal stress can indicate where the cavern wall damage can be caused by either shear or tensile stresses, or both. Figure 18 shows three-dimensional distribution of both factors at the end of simulation run (August 12, 2051). Simulation results suggest that the salt between 3300 and 3500 ft depth, where the vertical notch positive into the cavern is present, may experience dilatancy-driven damage (damage factor < 1; zoom-in area in Figure 18A) or tension (positive maximum principal stress; zoom-in area in Figure 18B) even with sequential leaching operations. Note that the vertical notches positive into the cavern of BM105 are still present because the cavern has not been fully developed, so that partial drawdowns leaching out some of that notch may improve stress state along the cavern wall.

4.3.2. BM108

Figures 19A and 19B show the minimum value of the damage factor and maximum value of the maximum principal stress at any point around the cavern BM108, respectively, as a function of time through five drawdowns. Two model results are compared; one from an old model with MDC salt model (dashed lines) and another from a new model updated with a new cavern geometry based on recent sonar data, MDV salt model, and a new cavern pressure history (solid lines).

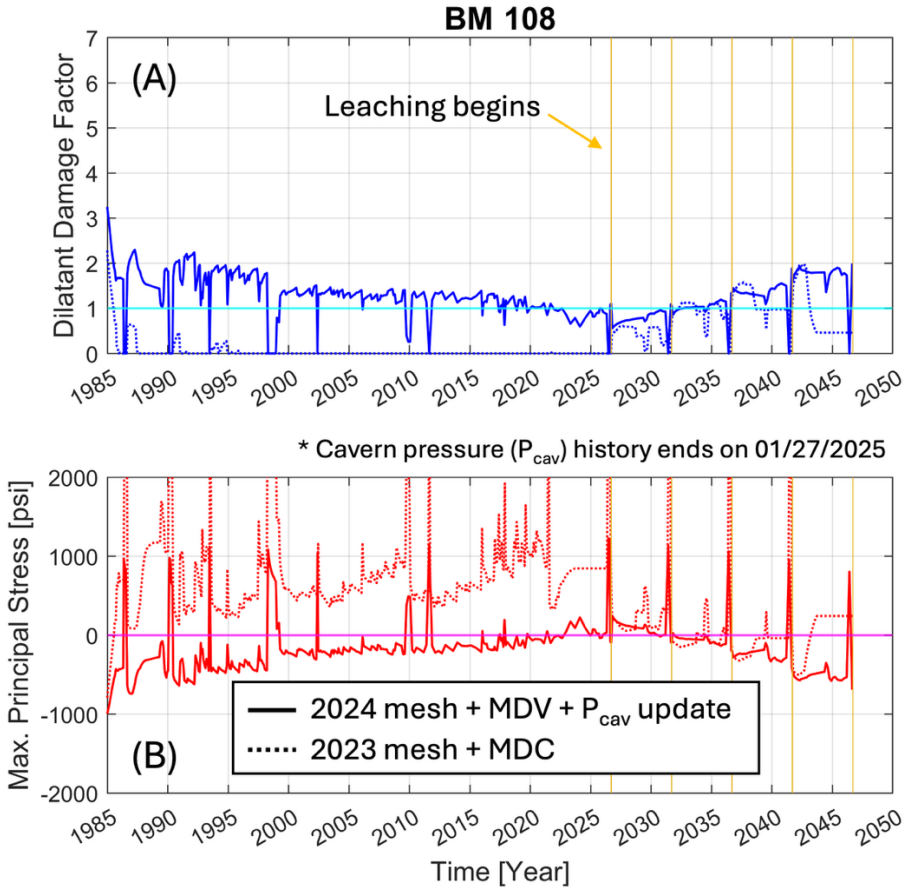

Figure 19. Stress-related damage analysis of BM108. (A) Predicted minimum damage factor for BM108 and (B) maximum principal stress in salt surrounding BM108. The dashed lines are for MDC model results, while solid lines are for MDV model results.

The new model predicts low values of dilatant damage factor are observed only near the end of operations and at the 1st leaching operation (solid line in Figure 19A) that were not observed in the old model (dashed line in Figure 19A). Subsequent leaching operations generate no excessive dilatant stress while the low damage factor values are observed only for a brief period coincident with a workover. These occurrences are not believed to be significant enough to cause microcracking in the salt of a magnitude that would affect cavern stability On the other hand, the maximum principal stresses stay below zero during the whole operation history (solid line in Figure 19B), which means that these occurrences are not believed to be significant enough to cause tension-driven microcracking in the salt of a magnitude that would affect cavern stability.

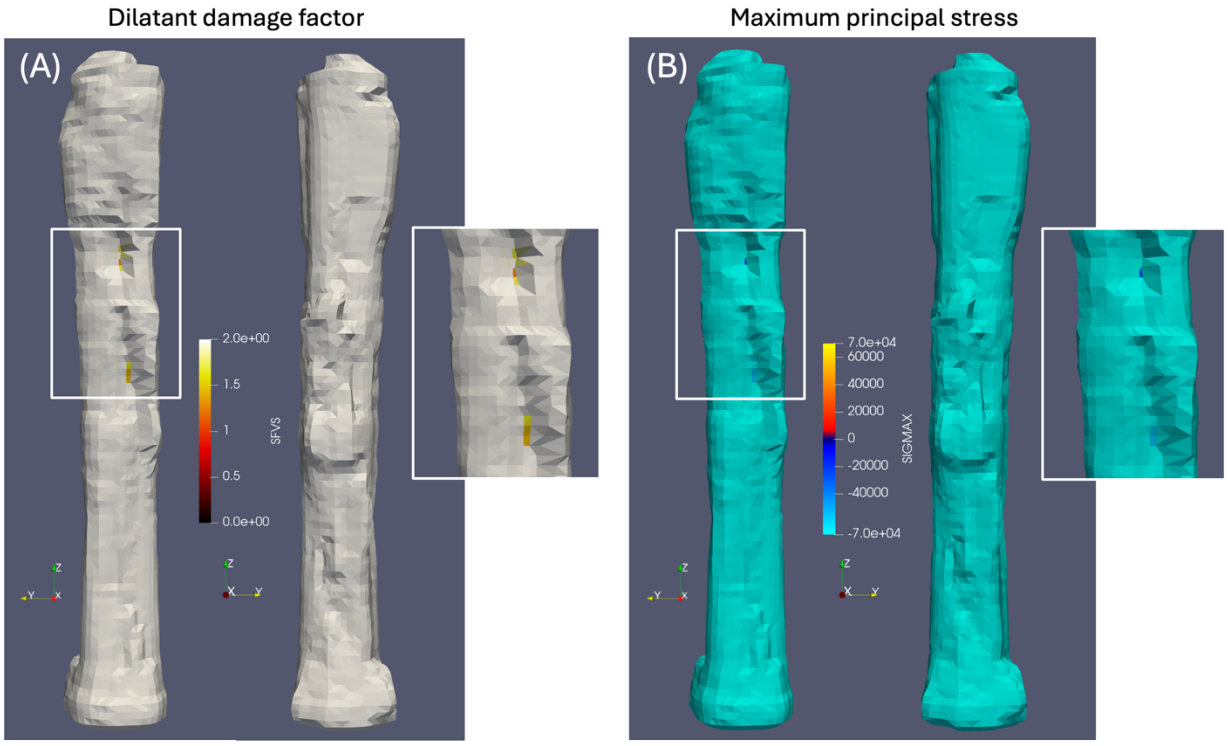

Figure 20. Three-dimensional distribution of (A) dilatant damage factor and (B) maximum principal stress on the BM108 cavern wall at the end of simulation run (August 12, 2051).

The spatial distribution of dilatant damage factor and maximum principal stress can indicate where the cavern wall damage can be caused by either shear or tensile stresses, or both. Figure 20 shows three-dimensional distribution of both factors at the end of simulation run (August 12, 2051). The minimum value of dilatant damage factor and maximum value of maximum principal stress occur at the same numerical element within a floor of the cavern, shown as orange and dark blue elements in Figures 20A and 20B, respectively. No excessive dilatant damage factors and maximum principal stresses are observed at other elements of BM108. A close examination reveals that the stress state indicating the potential of damage occurs at the element at the vertical notches positive into the cavern of BM105. Partial drawdowns leaching out some of that notch may improve stress state along the cavern wall. Hence, these occurrences are not believed to be significant enough to cause shearing- and/or tension-driven damage in the salt of a magnitude that would affect cavern stability.

4.3.3. BM109

Figures 21A and 21B show the minimum value of the damage factor and maximum value of the maximum principal stress at any point around the cavern BM109, respectively, as a function of time through five drawdowns. Two model results are compared; one from an old model with MDC salt model (dashed lines) and another from a new model updated with a new cavern geometry based on recent sonar data, MDV salt model, and a new cavern pressure history (solid lines).

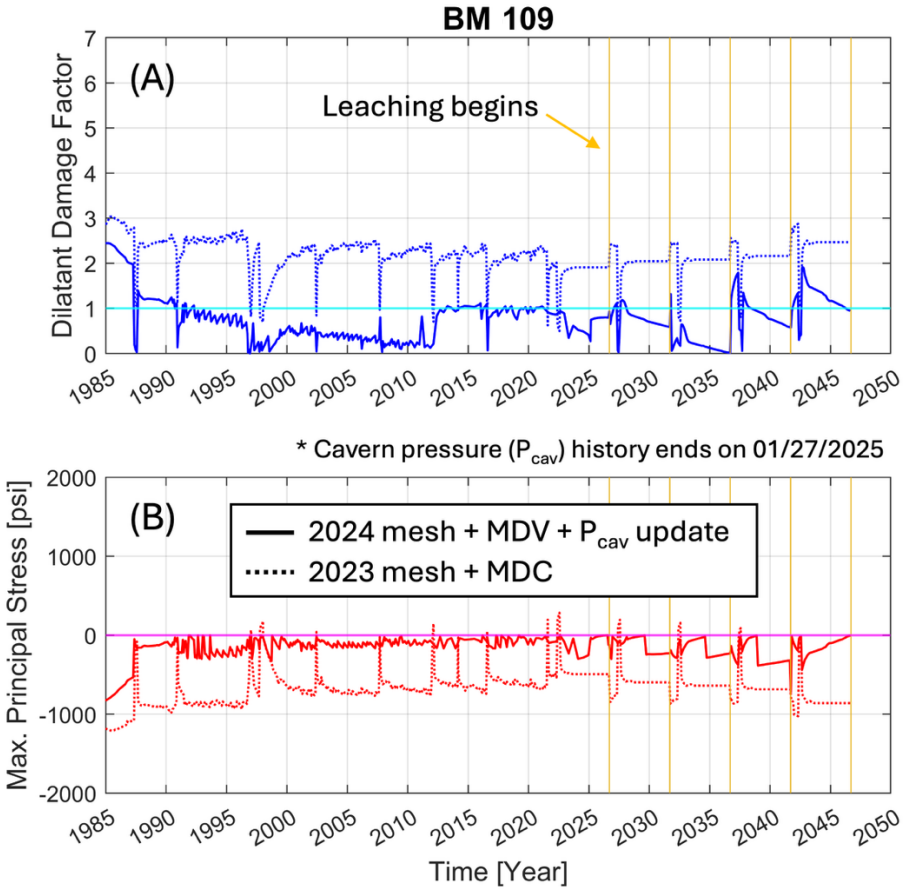

Figure 21. Stress-related damage analysis of BM109. (A) Predicted minimum damage factor for BM109 and (B) maximum principal stress in salt surrounding BM109. The dashed lines are for MDC model results, while solid lines are for MDV model results.

The new model predicts low values of dilatant damage factor less than 1 are observed during almost whole operation periods (solid line in Figure 21A) that were not observed from the old model. This result suggests that the update of model setting, implementing a recent cavern geometry and low-stress creep mechanism, may increase the potential of shearing-induced failure, even though subsequent leaching operations may enhance the cavern stability (e.g. values of dilatant damage factor > 1 after the 3rd leaching). On the other hand, the maximum principal stresses stay below zero, even quite close to zero (solid line in Figure 21B), which means that these occurrences are not believed to be significant enough to cause tension-driven microcracking in the salt of a magnitude that would affect cavern stability.

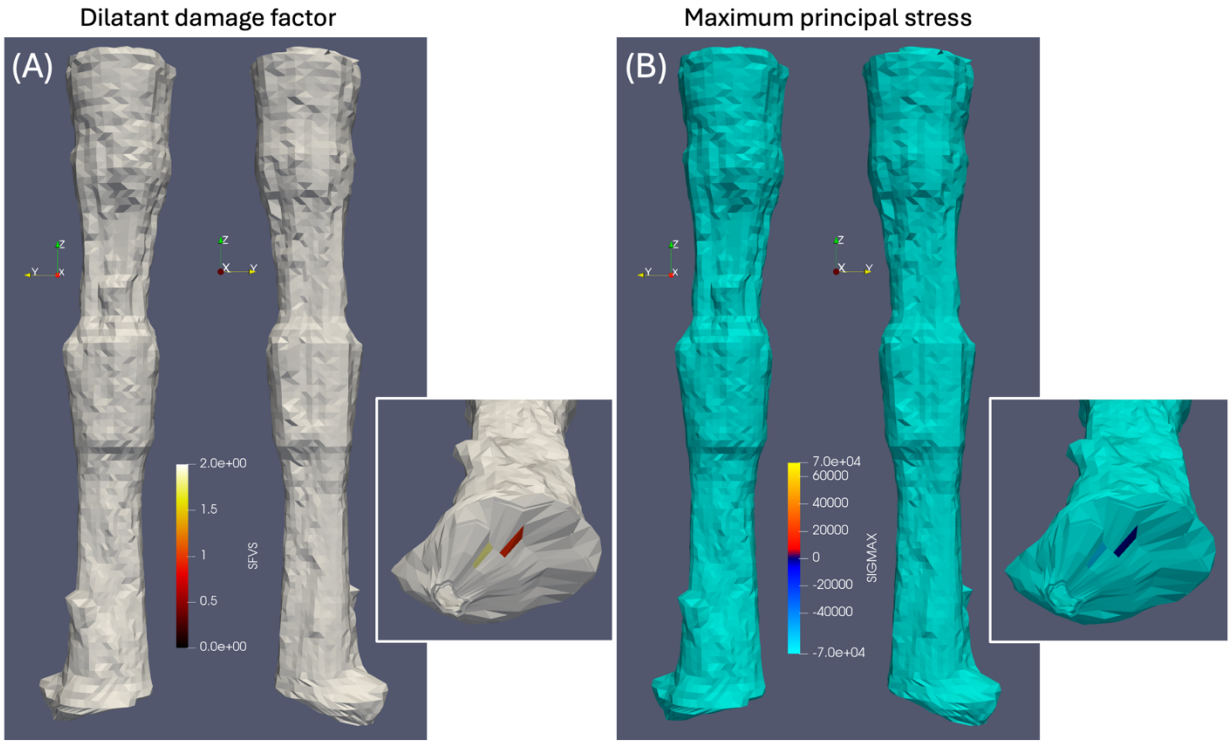

Figure 22. Three-dimensional distribution of (A) dilatant damage factor and (B) maximum principal stress on the BM109 cavern wall at the end of simulation run (August 12, 2051).

The spatial distribution of dilatant damage factor and maximum principal stress can indicate where the cavern wall damage can be caused by either shear or tensile stresses, or both. Figure 22 shows three-dimensional distribution of both factors at the end of simulation run (August 12, 2051). The minimum value of dilatant damage factor and maximum value of maximum principal stress occur at the same numerical element within a floor of the cavern, shown as red and navy elements in Figures 22A and 22B, respectively. No excessive dilatant damage factors and maximum principal stresses are observed at other elements consisting of the top and side boundaries of BM109. A close examination reveals that the extreme stress states occur at the element of the cavern floor (not located at the edge of the cavern floor), where there are sharp corner and excessive elongation in the mesh. The mesh geometry at this location is likely creating an artificially high stress concentration that exaggerates the stress at the bottom of the cavern. Hence, these occurrences are not believed to be significant enough to cause shearing-driven damage in the salt of a magnitude that would affect cavern stability.

4.4. Available Drawdown Limit Estimate Based on Geomechanics

The estimates for the available drawdowns for each of the Bryan Molund caverns have been updated based on the recently upgraded Bryan Mound geomechanical model. The new estimates for Bryan Mound are summarized in Table 8. All Bryan Mound Phase 2 caverns except BM105, 108, and 109 are predicted to have five available drawdowns remaining from the updated Bryan Mound geomechanics analysis. As described in Section 4.3, the damage potentials of BM105 and BM108 are observed at the vertical notches positive into the cavern because of immature cavern shape. Partial

drawdowns leaching out some of that notch may improve stress state along the cavern wall. For BM109, the extreme stress states occur at the computational element of the cavern floor (not located at the edge of the cavern floor) that represents the sharp angle changes observed from recent sonar data. This stress concentration may be resolved by implementing a new mesh technique, such as local refinement.

Table 8. Updated number of available drawdowns for Bryan Mound Phase 2 caverns.

Phase 2 cavern	Number		Description	Figure
	2018	2025		
101	5	5		
102	5	5		
103	2	5	Increase	
104	3	5	Increase	
105	2	2	Partial leaching will resolve the failure potential	17, 18
106	5	5		
107	5	5		
108	2	4	Partial leaching will resolve the failure potential	19, 20
109	3	3	A new numerical mesh technique can be a solution	21, 22
110	5	5		
111	5	5		
112	5	5		
113	5	5		
114	5	5		
115	5	5		
116	5	5		

5. CONCLUSIONS AND RECOMMENDATIONS

The results of the computational analyses lead to the following conclusions regarding the model itself, and the conditions of the caverns at Bryan Mound:

- The new multi-mechanism deformation viscoplastic (MDV) salt creep model has been implemented to the Bryan Mound geomechanical simulation that adds both steady-state and transient creep mechanisms at low-stress states for the geomechanical analysis.
- The sonar-based update of realistic cavern geometries to the computational mesh has contributed to identification of specific cavern regions, such as BM105, which can experience long-term dilatant and tensile stress conditions due to their geometries.
- The set of salt creep model properties for the MDV model are calibrated based on CAVEMAN-derived data of the cavern volume closure with a series of sensitivity tests with variation in the structure factor of "steady-state mechanism 0" (A_0 ≡ steady-state creep parameter at a low equivalent stress condition) within the reasonable range of A_0 for the domal salt.
- The simulation results of caprock damage model support a potential physical mechanism of caprock deformation induced by damage that may provide insight as to the cause of the wellbore failure. The partial damage of the caprock will localize the stress perturbation, such that a localized area of high stress may induce substantial deformation compared to other areas.
- The updated Bryan Mound model re-evaluates the potential of stress-related damage based on the evolution of dilatant and tensile stresses around certain caverns, including BM105, 108 and 109, through planned workover and drawdown activities.
- The number of available drawdowns for Phase 2 caverns is updated based on geomechanics analyses using recently updated Bryan Mound model.

The new model represents a more realistic assessment of the behavior of the Bryan Mound site. However, a significant amount of uncertainty still exists regarding several aspects of the computational model, and how they pertain to operational issues at the site. The types of uncertainty include the following items which will be addressed in future work:

- Implementing hydrological and mechanical properties of the caprock measured from the laboratory tests on core samples from the Bryan Mound site.
- Using the existing mesh but implementing different workover scenarios to test hypotheses of observed sympathetic behavior in one cavern when a nearby cavern undergoes a workover.
- Integrating different meshing techniques (e.g. local refinement or tetrahedral mesh) to represent the cavern geometry more realistically as well as to improve the computational efficiency by reducing the high aspect ratio of many elements due to the unusual cavern geometry.
- Adding an actual well structure into the current computational domain and/or developing a local model to look into the location-specific geomechanical behavior of the cavern and surrounding formation.
- Creating differently-shaped "onion skin" layers based on sonars or SANSMIC simulations will illustrate the leaching effects of partial drawdowns, which are much more the normal operating mode than a full bottom-to-top drawdown. Such partial drawdown scenarios will

be important for providing guidance to the DOE for tracking the available drawdown capacity for each cavern.

REFERENCES

[1] Ballard, S. and B.L. Ehgartner, 2000. *CaveMan Version 3.0: A Software System for SPR Cavern Pressure Analysis*, SAND2000-1751, Sandia National Laboratories, Albuquerque, New Mexico.

[2] Blacker, T.D., S.J. Owen, M.L. Staten, W.R. Quadros, B. Hanks, B.W. Clark, R.J. Meyers, C. Ernst, K. Merkley, R. Morris, C. McBride, C. Stimpson, M. Plooster, & S. Showman, 2016. *CUBIT Geometry and Mesh Generation Toolkit 15.2 User Documentation,* SAND2016-6850R, Sandia National Laboratories, Albuquerque, New Mexico.

[3] Ehgartner, B.L., 2004. *Incorporation of Compressibility Model and other enhancements/ upgrades into Caveman*, Letter to R.E. Myers, DOE-SPR, March 31, 2004, Sandia National Laboratories, Albuquerque, New Mexico.

[4] Ehgartner, B.L., 2009. *Subtask 1.3 Activity A4 Re-Optimization of Caveman Parameters*, Letter to R.E. Myers, DOE-SPR, April 29, 2009, Sandia National Laboratories, Albuquerque, New Mexico.

[5] Hansen, F. D., 2014. Micromechanics of Isochoric Salt Deformation. In: *48th US Rock Mechanics/Geomechanics Symposium*. American Rock Mechanics Association.

[6] Hogan, R.G., ed., 1980. Strategic Petroleum Reserve (SPR) Geological Site Characterization Report: Bryan Mound Salt Dome, SAND80-7111. Sandia National Laboratories, Albuquerque, NM.

[7] Keplinger and Associates, 1980. "Report of Investigations on Cavern #3, Bryan Mound Strategic Petroleum Reserve, Freeport, Texas," for Dravo Utility Constructors Inc. and U.S. Department of Energy, New Orleans, Louisiana, August 30, 1980.

[8] Kirby, C.L. and A.S. Lord, 2015. *Sulphur Extraction at Bryan Mound,* SAND2015-6827, Sandia National Laboratories, Albuquerque, New Mexico.

[9] Lama, R.D. and V.S. Vutukuri, 1978. *Handbook on Mechanical Properties of Rocks – Testing Techniques and Results*, Series on Rock and Soil Mechanics, Vol. 3, No.2, Trans Tech Publications.

[10] Lord, A.S., 2007. "An Updated Three-Dimensional Site Characterization Model of the Bryan Mound Strategic Petroleum Reserve Site, Texas," Letter Report to W. Elias, DOE PMO, November 5, 2007.

[11] kMunson, D.E., 1998. *Analysis of Multistage and Other Creep Data for Domal Salts*, SAND98-2276, Sandia National Laboratories, Albuquerque, New Mexico.

[12] Neal, J.T., T.R. Magorian, and S. Ahmad, 1994. *Strategic Petroleum Reserve (SPR) Additional Geologic Site Characterization Studies Bryan Mound Salt Dome, Texas*, SAND94-2331. Sandia National Laboratories, Albuquerque, New Mexico.

[13] Park, B.Y., C.G. Herrick, B.L. Ehgartner, M.Y. Lee and S.R. Sobolik, 2006. Numerical simulation evaluating the structural integrity of SPR caverns in the Big Hill salt dome. *In Proceedings of the 41st U.S. Symposium on Rock Mechanics: "50 Years of Rock Mechanics – Landmarks and Future Challenges,"* ARMA06-924, Golden, Colorado, June 17-21, 2006.

[14] Park, B. Y., B.L. Roberts, and S.R. Sobolik. 2017. Construction of hexahedral finite element mesh capturing realistic geometries of a petroleum reserve. *Journal of Finite Elements in Analysis and Design*, 135, 68–78. https://doi.org/10.1016/j.finel.2017.07.007.

[15] Park, B. Y., S.R. Sobolik, and C.G. Herrick. 2018. Geomechanical Model Calibration Using Field Measurements for a Petroleum Reserve. *Journal of Rock Mechanics and Rock Engineering*, ISSN 0723-2632, https://doi.org/10.1007/s00603-017-1370-4.

[16] Preece, D.S. and J.T. Foley, 1984. *Long-Term Performance Predictions for Strategic Petroleum Reserve (SPR) Caverns*, SAND83-2343, Sandia National Laboratories, Albuquerque, New Mexico.

[17] Rautman, C.A. and A.S. Lord, 2007. *Sonar Atlas of Caverns Comprising the U.S. Strategic Petroleum Reserve Volume 3: Bryan Mound Site, Texas*, SAND2007-6067, Sandia National Laboratories, Albuquerque, New Mexico.

[18] Reedlunn, B., 2018. *Enhancement to Munson-Dawson Model for Rock Salt*, SAND2018-12601, Sandia National Laboratories, Albuquerque, New Mexico.

[19] Sierra Team, 2022. *Sierra/SolidMechanics 5.10 User's Guide*, SAND2022-12223, Sandia National Laboratories, Albuquerque, New Mexico.

[20] Sobolik, S.R. and B.L. Ehgartner, 2009a. *Analysis of Cavern Stability at the Bryan Mound SPR Site,* SAND2009-1986, Sandia National Laboratories, Albuquerque, New Mexico.

[21] Sobolik, S.R. and B.L. Ehgartner, 2009b. *Analysis of Cavern Stability at the West Hackberry SPR Site,* SAND2009-2194, Sandia National Laboratories, Albuquerque, New Mexico.

[22] Sobolik, S.R., 2010. "Geomechanical Analysis of the Bryan Mound SPR Site with Mining-Induced Damage in the Caprock," Letter Report to R. Myers, July 13, 2010.

[23] Sobolik, S.R. and B.L. Ehgartner, 2012a. *Analysis of the Stability of Cavern 3 at the Bryan Mound SPR Site,* SAND2012-1953, Sandia National Laboratories, Albuquerque, New Mexico.

[24] Sobolik, S.R. and B.L. Ehgartner, 2012b. Structural Integrity of Oil Storage Caverns at a Strategic Petroleum Reserve Site with Highly Heterogeneous Salt and Caprock. In *Proceedings of the 46th U.S. Rock Mechanics Symposium,* ARMA 12-189*,* Chicago, Illinois, June 24-27, 2012.

[25] Sobolik, S.R., 2014. *Current Recommendations Regarding ECP PM-00449, Baseline Remaining Drawdowns for all SPR Caverns*, Letter to Lisa Nicholson, May 8, 2014, DOE-SPR, Sandia National Laboratories. U.S. Strategic Petroleum Reserve.

[26] Sobolik, S.R. and A.S. Lord, 2014. Case Study of the Impact of Prior Cavern Abandonment on Long-Term Oil Storage at a Strategic Petroleum Reserve Site. In *Proceedings of the 48th U.S. Rock Mechanics Symposium,* ARMA 14-7002*,* Minneapolis, Minnesota, June 1-4, 2014.

[27] Sobolik, S.R., 2018. Analysis of cavern and well stability at the Bryan Mound SPR site using the M-D salt creep model, SAND2018-9708, Sandia National Laboratories, Albuquerque, NM USA.

[28] Stein, J.S. and C.A. Rautman, 2005. *Conversion of the Bryan Mound Geological Site Characterization Reports to a Three-Dimensional Model*, SAND2005-2009, Sandia National Laboratories, Albuquerque, New Mexico.

[29] Stewart, J.R. and H.C. Edwards, 2003. The SIERRA Framework for Developing Advanced Parallel Mechanics Applications. In: Biegler, L.T., Heinkenschloss, M., Ghattas, O., van Bloemen Waanders, B. (eds) Large-Scale PDE-Constrained Optimization. Lecture Notes in Computational Science and Engineering, vol 30. Springer, Berlin, Heidelberg. https://doi.org/10.1007/978-3-642-55508-4_18.

[30] Van Sambeek, L.L., J.L. Ratigan, and F.D. Hansen, 1993. *Dilatancy of Rock Salt in Laboratory Tests*, Int. J. Rock Mech. Min. Sci. & Geomech. Abstr. Vol. 30, No. 7, pp 735-738.

DISTRIBUTION:

Email—Internal

Name	Org.	Sandia Email Address
Donald Conley	8612	dconley@sandia.gov
Anna C. Snider Lord	8612	acsnide@sandia.gov
Dave L. Lord	8616	dllord@sandia.gov
Dave B. Hart	8612	dbhart@sandia.gov
Hannah Maurer	8612	hgmaure@sandia.gov
Tonya S.A. Ross	8612	tsross@sandia.gov
Byoung Yoon Park	8612	bypark@sandia.gov
Technical Library	1911	sanddocs@sandia.gov

Email—External

Name	Company Email Address	Company Name
Diane Willard	diane.willard@spr.doe.gov	U.S. Department of Energy

This page left blank

Sandia National Laboratories

Sandia National Laboratories is a multimission laboratory managed and operated by National Technology & Engineering Solutions of Sandia LLC, a wholly owned subsidiary of Honeywell International Inc. for the U.S. Department of Energy's National Nuclear Security Administration under contract DE-NA0003525.